Hierarchical Mamba Meets Hyperbolic Geometry: A New Paradigm for Structured Language Embeddings

Anonymous authors
Paper under double-blind review

Abstract

Selective state-space models excel at long-sequence modeling, but their capacity for language representation – in complex hierarchical reasoning – remains underexplored. Most large language models rely on *flat* Euclidean embeddings, limiting their ability to capture latent hierarchies. To address this, we propose *Hierarchical Mamba (HiM)*, integrating efficient Mamba2 with hyperbolic geometry to learn hierarchy-aware language embeddings for deeper linguistic understanding. Mamba2-processed sequences are projected onto the Poincaré ball or Lorentzian manifold with "learnable" curvature, optimized with a hyperbolic loss. Our HiM model facilitates the capture of relational distances across varying hierarchical levels, enabling effective long-range reasoning for tasks like mixed-hop prediction and multi-hop inference in hierarchical classification. Experimental results show both HiM variants effectively capture hierarchical relationships across four linguistic and medical datasets, surpassing Euclidean baselines, with HiM-Poincaré providing fine-grained distinctions with higher h-norms, while HiM-Lorentz offers more stable, compact, and hierarchy-preserving embeddings-favoring robustness.[1]

1 Introduction

Large language models (LLMs), such as Transformers (Vaswani et al., 2017) and BERT (Devlin et al., 2019), typically encode input sequences into a *flat* Euclidean space. However, they struggle to capture the hierarchical and tree-like structures inherent in natural language (Chomsky, 1965), often leading to distortions at different levels of abstraction and specificity (Nickel & Kiela, 2017; Ganea et al., 2018). Moreover, transformer-based encoders face significant computational overhead due to the quadratic complexity of the attention mechanism (Vaswani et al., 2017). This limitation becomes particularly evident when dealing with hierarchical data (e.g., text ontologies, brain connectome (Ramirez et al., 2025; Baker et al., 2024)) with exponentially expanding structure. State-space models, starting with the Structured State Space (S4) model (Gu et al., 2021), have shown exceptional scalability for long-sequence modeling. Mamba's selective mechanism (Gu & Dao, 2023) dynamically prioritizes relevant information, achieving state-of-the-art performance in tasks with long-range dependencies. Mamba2 refines the original Mamba model for long-range sequence tasks by introducing a duality between state-space computations and attention-like operations, enabling the model to function as either an SSM or a structured, "mask-free" form of attention (Dao & Gu, 2024).

Recently, leveraging hyperbolic geometry as the latent representation space in machine learning models has shown great promise for learning meaningful hierarchical structures (Nickel & Kiela, 2018; Peng et al., 2021; Petrovski, 2024). The Poincaré disk and Lorentz model are two prevalent representations of hyperbolic space. The Poincaré disk model is often favored for its conceptual simplicity (bounded in a unit ball). However, the Lorentz model (with unbounded infinite space) offers a closed-form distance function, but requires careful handling of numerical functions dealing with space-like dimensions and a time-like dimension using exponential mapping and logarithmic mapping (Peng et al., 2021). These numerical considerations are critical because the improper handling of the time-like coordinate in Lorentz models can lead to manifold violations, requiring specialized projection techniques (Fan et al., 2024; Liang et al., 2024). Existing hyperbolic LLM architectures (He et al., 2024b; Peng et al., 2021) often rely on Transformer blocks and apply a simple

---

Poincaré disk model, leading to $O(L^2)$ complexity that becomes prohibitive for long sequences typical in deep hierarchies. A key challenge in implementing hyperbolic models is tuning the curvature to maintain numerical stability, particularly in Lorentz parameterization.

In this paper, we introduce hyperbolic mamba with the Lorentz model, and compare it with its counterparts – *Poincaré model and Euclidean model*. To address the potential numerical instability in the Lorentz model (Mishne et al., 2023), we explicitly bound the embedding norms and employ curvature-constrained Maclaurin approximations for hyperbolic operations. HiM aims to achieve high-performance hierarchical classification by preserving relational hierarchies. It demonstrates scalability for processing long sequences without compromising on accuracy or computational efficiency. HiM's novelty lies in integrating a state-space model (Mamba2) with hyperbolic geometry, leveraging Mamba2's $O(L)$ complexity for efficient sequence modeling while preserving hyperbolic properties for hierarchical representation. Additionally, our HiM incorporates task-specific hyperbolic losses that explicitly enforce parent-child distance constraints in hyperbolic space, enabling end-to-end hierarchy learning without Euclidean biases and achieving significant F1 gains on multi-hop inference tasks. To support HiM's framework, we introduce **SentenceMamba-16M**, a compact, Mamba2-based large language model with 16 million parameters designed to generate high-quality sentence embeddings.

2 Related Works

Hyperbolic geometry has demonstrated strong potential in modeling hierarchical structures in both shallow and deep neural networks. Foundational works, such as Poincaré embeddings (Nickel & Kiela, 2017) and hyperbolic entailment cones (Ganea et al., 2018), showed their effectiveness in capturing hierarchical relationships in taxonomies with shallow neural networks. Moreover, hyperbolic manifolds have also been applied to encode hierarchies in graph-structured data (Liu et al., 2019; Chami et al., 2019). More recent efforts have extended hyperbolic representations to multimodal computer vision tasks, including visual and audio modalities (Yang et al., 2024c; Mandica et al., 2024), further demonstrating their strength in capturing both hierarchical structure and uncertainty.

However, hyperbolic approaches in language modeling remain limited. As an early approach to hyperbolic word embeddings, Dhingra et al. (2018) provided an important early step by reparameterizing Poincaré embeddings for GRU-based sequence modeling. This approach eliminated projection steps and supported both shallow and parametric encoders, but it was ultimately limited by its shallow representations, which restricted its expressive power and ability to capture long-range dependencies. More recent research has extended these concepts to transformers and their variants (He et al., 2024b; Chen et al., 2021; 2024). These approaches enable effective prediction of subsumption relations and transitive inferences across hierarchy levels using hyperbolic embeddings, providing a principled framework for encoding syntactic dependencies through geodesic distances. However, Hyperbolic BERT exhibits high computational cost than standard BERT due to the complexity of hyperbolic operations (Chen et al., 2024). To improve efficiency, recent works have explored fine-tuning LLMs directly in hyperbolic space with the Low-Rank Adaptation (LoRA) technique (Hu et al., 2022). For example, HoRA (Yang et al., 2024a) and HypLoRA (Yang et al., 2024b) apply LoRA to the hyperbolic manifold, allowing parameter-efficient fine-tuning while capturing complex hierarchies. These methods show strong gains—up to 17.3% over Euclidean LoRA. However, these models usually assume a constant curvature, which may not be optimal for all data, and can suffer from numerical instability due to the exponential and logarithmic mappings required to transition between Euclidean and hyperbolic spaces (López & Strube, 2020).

Limitations in Current Approaches and Our Contribution: Despite significant progress, most existing methods either exploit only partial hyperbolic representations (e.g., using adapters or static embeddings) or rely heavily on attention-based architectures that scale poorly with long sequences and deep hierarchies. For instance, Poincaré GloVe (Tifrea et al., 2018) is limited to word embeddings, failing to capture dynamic, context-dependent relationships, while Hyperbolic BERT (Chen et al., 2024) and HiT (He et al., 2024b) introduce significant computational overhead, especially for long sequences. Similarly, probing BERT's embeddings in a Poincaré ball (Chen et al., 2021) to analyze hierarchical structures, but their diagnostic approach does not train a new model for hierarchical reasoning tasks like HiM. Methods, such as HoRA (Yang et al., 2024a) and HypLoRA (Yang et al., 2024b), only introduce hyperbolic geometry through adapter modules

added post hoc to standard transformer backbones. These methods inherit the architectural inefficiencies of transformers but cannot fully encode hierarchy directly within the hyperbolic latent space. Building on the strengths and limitations discussed above, we propose *Hierarchical Mamba (HiM)* as a novel framework for long-range hierarchical reasoning. Our contributions can be summarized as follows:

- **Direct hyperbolic integration:** Unlike HiT (He et al., 2024b), which fine-tunes pretrained Euclidean embeddings (all-MiniLM-L6-v2) in low-curvature hyperbolic space ($\mathcal{K} = -1/384$), or HoRA/HypLoRA (Yang et al., 2024a;b), which adds hyperbolic LoRA adapters post-hoc to frozen Euclidean transformer backbones, HiM trains a Mamba2 encoder from scratch directly in hyperbolic space with learnable curvature, operating at strong negative curvature ($\mathcal{K} = -1.0$) on both Poincaré and Lorentz manifolds without inheriting Euclidean biases.
- **SentenceMamba-16M:** We develop the first Mamba2-based sentence encoder (SentenceMamba-16M, 16M parameters) with specialized pooling strategies and hyperbolic projection interfaces tailored for sentence representation.
- **Stabilized hyperbolic operations:** HiM addresses numerical instability in Lorentzian manifolds using curvature-bounded Maclaurin approximations for hyperbolic functions, ensuring robust training for deep hierarchies and higher curvatures.
- **Hyperbolic losses:** Building on HiT's clustering and centripetal losses (He et al., 2024b), we introduce curvature-aware dynamic margin scaling that adapts margins proportionally with new radius updated as per learned hyperbolic radius, and variance regularization in the centripetal loss to prevent norm collapse at high curvature.

3 Methodology

Hyperbolic geometry, characterized by negative curvature $\mathcal{K} = -1/c$, is well-suited for hierarchical data due to its exponential growth properties, modeled using the Poincaré ball or Lorentz model (Nickel & Kiela, 2017; 2018). Mamba2, a state-space model (SSM), offers efficient sequence modeling with linear complexity, using structured state-space duality to balance SSM and attention-like operations (Dao & Gu, 2024).

3.1 Hyperbolic Mamba (HiM)

The overall framework of HiM, including the integration of Mamba2 blocks and hyperbolic projections is shown in Figure 1. Firstly, the raw text is tokenized into a sequence of tokens; these token IDs are mapped into embedded tokens resulting in token IDs of shape $[B, L, D, N]$, where B is the batch size ($B = 256$), L is the sequence length ($L = 128$), and D is the embedding dimension ($D = 384$), and N is the state dimension ($N = 96$). These token embeddings are processed through four Mamba2 blocks. Given an input sequence $\mathbf{x}_{1:L} \in \mathbb{R}^{L \times D}$, the discrete-time SSM at each timestep t is defined by:

$$\mathbf{h}_t = \mathbf{A}_t \mathbf{h}_{t-1} + \mathbf{B}_t \mathbf{x}_t, \quad \mathbf{y}_t = \mathbf{C}_t \mathbf{h}_t \tag{1}$$

where $\mathbf{h}_t \in \mathbb{R}^N$ is the hidden state at timestep t, and the selective mechanism makes the matrices $\mathbf{A}_t, \mathbf{B}_t, \mathbf{C}_t$ input-dependent (see Appendix A.2 for detailed formulation of Mamba2). Alanis-Lobato et al. (2016) focuses on efficient embedding of complex networks into hyperbolic space using the network Laplacian, achieving a computational complexity of $O(N^2)$ and enabling the analysis of large networks in seconds. This highlights the importance of computational efficiency in scaling hyperbolic models, a principle that HiM extends by Mamba2 blocks (Equations 18 and 21) to achieve linear-time complexity $O(L)$, making it particularly suited for long sequences and deep hierarchical language structures. In the Mamba2 blocks, the inputs $\mathbf{x}_t$ having 384 dimensions are projected into the intermediate state I having 768 dimensions using a linear transformation ($D : 384 \rightarrow I : 768$).

The $\mathbf{x}'_t$ component undergoes a convolution operation with a kernel size of 4. A SiLU activation function follows this operation for non-linearity. In the output projection, the intermediate state dimensions are projected back to their original embedding dimension $I : 768 \rightarrow D : 384$ for compatibility with downstream tasks. The SentenceMamba-16M model, central to HiM, is randomly initialized with Kaiming normal weights instead of pretrained weights, enabling it to learn hierarchical structures directly from training data in hyperbolic space without any biases. The SentenceMamba-16M model is trained using Triplet Contrastive Loss, which brings embeddings of positive pairs closer together while pushing apart embeddings of other
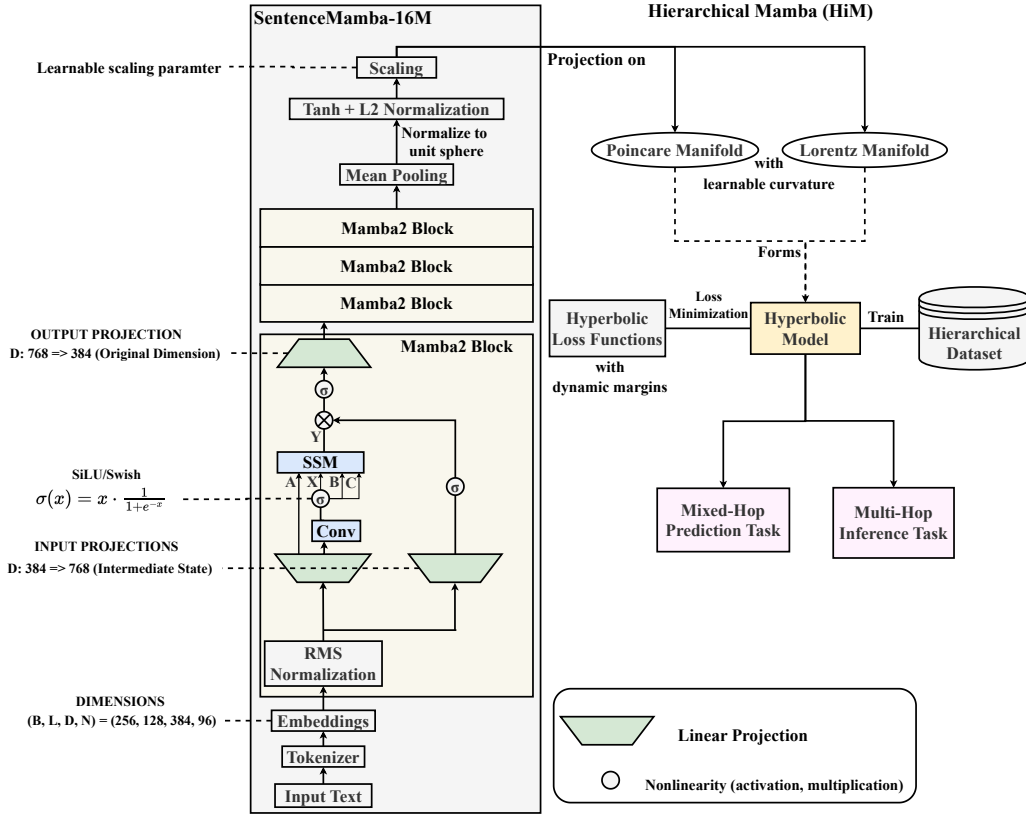
Figure 1: Overview of the Hierarchical Mamba (HiM) model, integrating Mamba2 blocks with hyperbolic projections to the Poincaré ball (via tangent-based mapping) and Lorentzian manifold (via cosine/sine-based mapping), enabling efficient and hierarchy-aware language embeddings for long-range reasoning tasks.

sentences in the batch. This loss function has proven effective in prior works involving hierarchical embedding (Schroff et al., 2015; He et al., 2024b). After normalizing each embedding to unit length, we measure the pairwise cosine similarity as $\text{sim}(i,j) = \mathbf{e}_i \cdot \mathbf{e}_j$, where each embedding $\mathbf{e}_i$ and $\mathbf{e}_j$ belong to $\mathbf{e} \in \{\mathbf{e}_1, \mathbf{e}_2, \ldots, \mathbf{e}_n\}$. We then calculate the contrastive loss for the batch by constructing a similarity matrix from the similarity scores across nodes. The sentence embeddings are constrained using hyperbolic tangent activation followed by L2 normalization to ensure numerical stability:

$$\mathbf{u} = \text{normalize}(\tanh(s)), \tag{2}$$

where $\mathbf{s}$ is the mean-pooled embedding from the Mamba2 blocks and $\text{normalize}(\cdot)$ denotes L2 normalization. This operation reduces the sequence to a single fixed-size vector, representing the pooled features of the entire input sequence normalized to unit sphere.

To ensure numerical stability during hyperbolic projection, we apply norm scaling with a learnable parameter γ:

$$\mathbf{h} = \begin{cases} \gamma \cdot \mathbf{u}, & \text{for Poincaré,} \\ \gamma \cdot \text{clamp}(\mathbf{u}, -8, 8), & \text{for Lorentz.} \end{cases} \tag{3}$$

This approach mitigates numerical overflow and enhances training stability. The interplay between the norm scaling parameter γ and curvature $\mathcal{K} = -1/c$ is mathematically significant. When we scale embeddings by γ before projection, it effectively modulates the spread of embeddings in the hyperbolic space. Our model learns both the curvature parameter c and a scaling factor γ that together determine the optimal geometry for representing hierarchical relationships. This dual learning approach provides flexibility in adapting the hyperbolic space to the structural complexity of the data while maintaining numerical stability. Then the

vector h is mapped to a point e in hyperbolic space. The general form for a Poincaré ball with radius $r = \sqrt{c}$ (curvature $\mathcal{K} = -1/c = -1/r^2$) is:

$$e_P = \sqrt{c} \cdot \tanh\left(\frac{\|\mathbf{h}\|}{\sqrt{c}}\right) \cdot \frac{\mathbf{h}}{\|\mathbf{h}\|}, \tag{4}$$

where $\|h\|$ is the norm of embedding vector h. This scaling ensures the vector lies within the unit ball. This yields the final sentence embedding e with values constrained between -1 and 1 (indicating a positive or negative parent), allowing us to project the embedding onto the Poincaré Ball manifold.

We also project it onto the Lorentzian manifold as it yields richer features in a more convenient original hyperbolic space. The pooled embeddings are instead mapped to the Lorentzian manifold using:

$$e_L = \begin{bmatrix} \sqrt{c} \cdot \cosh\left(\frac{\|\mathbf{h}\|}{\sqrt{c}}\right) \\ \sqrt{c} \cdot \sinh\left(\frac{\|\mathbf{h}\|}{\sqrt{c}}\right) \cdot \frac{\mathbf{h}}{\|\mathbf{h}\|} \end{bmatrix}. \tag{5}$$

Here, $\|h\|$ is the norm distance of embedding vector h, $\sqrt{c}$ is the radius of the hyperbolic space; $\mathcal{K} < 0$ ensures hyperbolic geometry. For the Lorentz mapping we let $z = \|\mathbf{h}\|/\sqrt{c}$ in Equation 5. The **cosh, sinh** functions are the Hyperbolic cosine and sine functions used to compute projections. The first term $\sqrt{c} \cdot \cosh\left(\frac{\|\mathbf{h}\|}{\sqrt{c}}\right)$ in the Lorentz projection is the time-like dimension. The remaining components $\sqrt{c} \cdot \sinh\left(\frac{\|\mathbf{h}\|}{\sqrt{c}}\right) \cdot \frac{\mathbf{h}}{\|\mathbf{h}\|}$ are the space-like dimension. This step is crucial for hyperbolic geometry as it ensures the embeddings are bounded, enabling seamless projection onto the Lorentzian manifold.

While the Lorentz projection typically uses exact hyperbolic functions, we stabilize the training even more by approximating cosh and sinh via their Maclaurin (Taylor) expansions for $|z| < 10^{-3}$. By substituting truncated polynomial expansions, we limit overflow and hence solve the problem of exploding gradients.

$$\cosh(z) = 1 + \frac{z^2}{2!} + \frac{z^4}{4!} + \cdots; \qquad \sinh(z) = z + \frac{z^3}{3!} + \frac{z^5}{5!} + \cdots. \tag{6}$$

Then, the first (time-like) coordinate and the remaining (space-like) coordinates from Equation 5 become:

$$\mathbf{e_L} \approx \begin{bmatrix} \sqrt{c}\left(1 + \frac{z^2}{2} + \frac{z^4}{24} + \cdots\right) \\ \sqrt{c}\left(z + \frac{z^3}{6} + \frac{z^5}{120} + \cdots\right)\frac{\mathbf{h}}{\|\mathbf{h}\|} \end{bmatrix}. \tag{7}$$

To fully exploit the hyperbolic structure of our model, we employ an advanced hyperbolic loss function for the HiM model optimization, which is a weighted combination of centripetal loss and clustering loss. These losses enhance the model's ability to effectively learn hierarchical relationships by optimally positioning and grouping the embeddings in a strongly hierarchical structure within the Hyperbolic manifold. Detailed equations for our hyperbolic loss are presented below, with the full calculation process provided in Appendix B.

Clustering Loss: This loss function clusters related entities and distances unrelated ones within the hyperbolic manifold, promoting the grouping of similar entities while preserving hierarchical separation.

$$\mathcal{L}_{\text{cluster}} = \sum_{(e,e^+,e^-) \in \mathcal{D}} \max(d_c(e, e^+) - d_c(e, e^-) + \alpha, 0). \tag{8}$$

Centripetal Loss: This loss function ensures that parent entities are positioned closer to the origin of the hyperbolic manifold than their child counterparts. This reflects the natural expansion of hierarchies from the origin to the boundary of the manifold, while preventing norm collapse through variance regularization.

$$\mathcal{L}_{\text{centri}} = \sum_{(e,e^+,e^-) \in \mathcal{D}} \max(\|e^+\|_c - \|e\|_c + \beta, 0) - \lambda_{\text{var}} \cdot \text{Var}(\{\|e\|_c, \|e^+\|_c\}). \tag{9}$$

Here, (e, e^+, e^-) represent the hyperbolic embeddings of a randomly selected anchor node, its positive parent node, and an unrelated negative node, respectively. $\|e\|_c$ or $d_c(e, 0)$ measures the distance from the origin to the hyperbolic embedding e in the Poincaré and Lorentzian manifold. $d_c(e, e^+)$ measures the distance between hyperbolic embeddings of node e and its positive parent node e^+. $d_c(e, e^-)$ measures the distance between node e and a negative node e^-. α and β denote margin parameters to enforce centripetal and clustering properties, respectively. λ_{var} is the variance regularization weight set to 0.002 in our experiments.

The Hyperbolic Loss $\mathcal{L}_{hyperbolic}$ is defined as the weighted sum of Centripetal Loss $\mathcal{L}_{centri}$ and Clustering Loss $\mathcal{L}_{cluster}$:

$$\mathcal{L}_{hyperbolic} = w_{ce}\mathcal{L}_{centri} + w_{cl}\mathcal{L}_{cluster}, \tag{10}$$

where w_{ce} and w_{cl} are weights that control the contribution of each loss component. To the base forms of clustering and centripetal losses, our implementation introduces **curvature-aware dynamic margin scaling**, where margins α and β scale proportionally with the learned radius $R = 1/\sqrt{c}$ to maintain geometric consistency as curvature adapts during training ($\alpha = 0.255 \times R$, $\beta = 0.0051 \times R$), and **variance regularization** $\mathcal{L}_{\text{var}} = -\text{Var}(\{\|e\|_c\})$ added to the centripetal loss to prevent norm collapse under strong curvature by encouraging diversity in hyperbolic norms. This loss ensures that the model maintains the hierarchical structure during training, with parent entities closer to the origin and related entities clustered together. The margins α and β in the clustering and centripetal losses (Equations 9 and 8) are implemented as dynamic parameters optimized during training to adaptively enforce the hierarchical constraints. The margins for the clustering and centripetal losses are adapted to the hyperbolic geometry by scaling proportionally with the radius $r = \sqrt{c}$, ensuring the loss functions remain geometrically consistent across different curvatures. These scaling factors were determined through empirical validation to maintain consistent separation properties as the model adapts its curvature during training. The clustering margin is intentionally larger to enforce robust hierarchical separation between related and unrelated entities, while the centripetal margin is smaller to allow fine-grained positioning of parent nodes closer to the origin relative to their children, reflecting the natural expansion of hierarchies in hyperbolic space. In all hierarchical classification tasks, hard negatives were chosen to sharpen the model's discrimination (Schroff et al., 2015). Rather than randomly sampling unrelated nodes, we select negative examples that are semantically close to the anchor (or positive) in embedding space. This training strategy forces the model to learn more subtle hierarchical distinctions, which is crucial for tasks such as "multi-hop inference". We observe that hard negatives lead to better generalization.

Following Chami et al. (2019), we optimize the learnable curvature parameter using the AdamW optimizer. This is justified because the curvature parameter itself is a scalar Euclidean variable controlling the hyperbolic manifold geometry, making AdamW both theoretically valid and empirically stable. To ensure numerical stability during training in hyperbolic space as the curvature adapts, we implement a geometric stabilization technique that periodically projects the model parameters back onto the manifold. Specifically, every 100 optimization steps, this stabilization counteracts numerical drift that can occur during curvature optimization, preventing embeddings from violating the constraints of the hyperbolic geometry and ensuring all distance computations remain well-defined throughout training.

4 Experiments

Dataset We compare our proposed HiM models with their Euclidean counterparts, evaluated across four ontology datasets (i.e., DOID, FoodOn, WordNet, and SNOMED-CT) varying in scale and hierarchical complexity.[2]. (1) DOID offers a structured representation of human diseases through "is-a" relationships (Schriml et al., 2012). (2) FoodOn is a detailed ontology that standardizes food-related terminology, covering ingredients, dishes, and processes for nutritional classification and dietary research. It uses a hierarchical structure and borrows from existing ontologies like LanguaL (Dooley et al., 2018). (3) WordNet is a well-known benchmark that organizes English nouns, verbs, and adjectives into synonym sets connected by hypernym-hyponym relationships (Miller, 1995). (4) SNOMED Clinical Terms (SNOMED-CT) is a comprehensive clinical terminology system used in electronic health records (EHRs). It organizes concepts (e.g., diagnoses, procedures, symptoms) into multiple hierarchies, linked by "is-a" and attribute relationships (Stearns et al., 2001). All datasets are derived from structured taxonomies and can be represented as directed acyclic graphs, where nodes denote entities and edges denote direct subsumption (i.e., parent-child) relations.

---

[2]Datasets are available from `https://zenodo.org/records/14036213` and see Table 3 in Appendix C for details

Implementation Details   We use 4 NVIDIA A100 GPUs with 80GB of memory each, distributed across a single compute node. Our model is implemented using the mamba-ssm library (Dao & Gu, 2024). To define and operate over hyperbolic manifolds, we use GeoOpt (Kochurov et al., 2020), while DeepOnto (He et al., 2024a) is employed to process and manage hierarchical structures in the ontology datasets. We leverage distributed data-parallel training with PyTorch's DistributedDataParallel wrapper (Paszke, 2019). Our models were trained for ten epochs using the AdamW optimizer with a linear warm-up learning rate over the first 100 steps (target learning rate set to $1e-4$), and weight decay of $1e-3$. The linear warm-up is followed by a constant learning rate $1e-4$. The maximum gradient norm is clipped to 1.0. We employ a combination of hyperbolic clustering loss and hyperbolic centripetal loss during pretraining, with weights of 1.0 and 1.0, respectively. Our model incorporates several learnable parameters, such as scaling factor γ (initialized to 0.01), curvature $\mathcal{K}$ (initialized to -1.0). We implement dynamic margin parameters for losses α and β, which depend on the updated curvature. We use a batch size of 256 per GPU. To regularize the model during training, a dropout rate of 0.2 is applied following each Mamba2 block. The detailed train/validation/test splits for mixed-hop prediction and multi-hop inference tasks, can be found from Table 3 in Appendix C.

Evaluation Tasks and Metrics   We evaluated our HiM models on two key tasks designed to assess its hierarchical reasoning capabilities in ontology completion and knowledge graph inference: (1) *multi-hop inference*, which involves predicting the existence of indirect relationships (e.g., "dog is a vertebrate") through transitive reasoning. (2) *mixed-hop prediction*, which focuses on estimating hierarchical distances between entities (e.g., 1-hop vs. 2-hop relations). Both tasks are formulated as classification problems based on hyperbolic distances. Detailed formulations are provided in Appendix D. We use three metrics for evaluation: F1 score, Precision, and Recall. Among them, the F1 score serves as the primary metric, as it provides a balanced measure of precision and recall, which is critical for hierarchical reasoning tasks. Following prior work on these datasets (He et al., 2024b), we exclude Accuracy due to its vulnerability to class imbalance, where negative samples significantly outnumber positive ones. During training, models are optimized using entity triplets (anchor, positive, negative) under a contrastive learning framework; however, evaluation is performed on entity pairs to directly assess subsumption prediction performance.

5   Results

We compare our proposed HiM models–HiM-Poincaré and HiM-Lorentz–against three Euclidean baselines on four hierarchical datasets for two main downstream tasks: mixed-hop prediction and multi-hop inference. The Euclidean baselines include: (1) **Pretrained SentenceMamba-16M**, trained on the SNLI dataset (Bowman et al., 2015); (2) **Finetuned (with pretrained weights)**, which continues training from the pretrained checkpoint on hierarchical datasets; and (3) **Trained from scratch**, which uses random initialization (Kaiming normal for weights, zero for biases) and is trained directly on hierarchical datasets in Euclidean space. Our HiM models share the SentenceMamba-16M backbone ($\approx$ 16M parameters), but incorporate learnable curvature and are trained from scratch without pretrained weights in hyperbolic space using both Poincaré and Lorentzian manifolds.

5.1   Comparison between HiM models and their Euclidean baselines

We present a comprehensive comparison of HiM-Poincaré, HiM-Lorentz, and their Euclidean baselines, including the pretrained SentenceMamba-16M, fine-tuned SentenceMamba-16M (with pretrained weights) and trained SentenceMamba-16M (trained from scratch on hierarchical datasets) in Table 1. Both HiM models were trained with learnable curvature parameter $\mathcal{K} = -1/c$. A deeper curvature (smaller radius $r =>$ smaller $c =>$ larger/deeper curvature $\mathcal{K}$) allows us to exploit the hierarchical structure of the Hyperbolic manifold much better, as the hyperbolic embeddings are confined in the conical manifold compact within a smaller radius. The average δ-hyperbolicity (Gromov, 1987) for each dataset measures the tree-likeness of the graph by calculating the maximum deviation from the four-point condition. Values closer to 0 indicate a more hierarchical structure (Adcock et al., 2013), making these datasets well-suited for hyperbolic embeddings. The corresponding δ-hyperbolicity scores for the four datasets are reported in Table 1, reflecting a descending order of hierarchy complexity: DOID $\rightarrow$ SNOMED-CT $\rightarrow$ WordNet $\rightarrow$ FoodOn. The experimental results illustrate that HiM-Lorentz model achieves more robust and stable performance (with extremely small variance) in terms of the F1, precision, and recall values for both mixed-hop prediction and multi-hop inference tasks across four datasets. Moreover, HiM-Lorentz outperformed the HiM-Poincaré variant on the multi-hop inference task for both the WordNet and SNOMED-CT datasets, both of which are relatively

large datasets and exhibit deeper hierarchies characterized by small δ-hyperbolicity. However, in the case of FoodOn—which also has *higher hyperbolicity*—the Poincaré-based model achieved better performance. To verify that the weak zero-shot performance of the pretrained Euclidean baseline is not merely an effect of small parameter scale, we additionally report inference-only baselines for substantially larger pretrained encoders in Appendix H.1.

Table 1: Performance comparison of Pretrained, Finetuned (with pretrained weights), Trained from scratch across Euclidean manifold, and HiM models across Hyperbolic manifolds on various datasets (with varying average δ-hyperbolicity). Pretrained SentenceMamba-16M is trained on SNLI; Finetuned (with pretrained weights) continues training from the pretrained checkpoint; Trained from scratch uses random initialization (Kaiming normal for weights, zero for biases). HiM models use learnable curvature for hyperbolic projections. The mean and standard deviation of F1, Precision and Recall scores were computed over five independent runs for each setting. (See details in Appendix F)

Metric	Euclidean ($\mathcal{K} = 0$)			Hyperbolic ($\mathcal{K} < 0$, learnable)	
	Pretrained	Finetuned (pretrained weights)	Trained from scratch	HiM-Poincaré	HiM-Lorentz
Mixed-hop Prediction (DOID) : Average δ-hyperbolicity = 0.0190					
F1	0.135 ± 0.022	0.744 ± 0.029	0.436 ± 0.043	0.795 ± 0.019	$\mathbf{0.821 \pm 0.003}$
Precision	0.087 ± 0.003	0.815 ± 0.013	0.776 ± 0.016	0.812 ± 0.020	$\mathbf{0.822 \pm 0.004}$
Recall	0.390 ± 0.207	0.685 ± 0.041	0.305 ± 0.040	0.780 ± 0.026	$\mathbf{0.820 \pm 0.007}$
Mixed-hop Prediction (FoodOn) : Average δ-hyperbolicity = 0.1852					
F1	0.125 ± 0.046	0.634 ± 0.011	0.550 ± 0.017	$\mathbf{0.836 \pm 0.031}$	0.827 ± 0.002
Precision	0.090 ± 0.009	0.760 ± 0.008	0.688 ± 0.008	0.841 ± 0.024	$\mathbf{0.852 \pm 0.007}$
Recall	0.330 ± 0.232	0.544 ± 0.019	0.459 ± 0.023	$\mathbf{0.831 \pm 0.033}$	0.803 ± 0.002
Mixed-hop Prediction (WordNet) : Average δ-hyperbolicity = 0.1438					
F1	0.135 ± 0.044	0.580 ± 0.015	0.615 ± 0.009	$\mathbf{0.824 \pm 0.024}$	0.823 ± 0.003
Precision	0.086 ± 0.014	0.702 ± 0.009	0.755 ± 0.018	$\mathbf{0.853 \pm 0.023}$	0.828 ± 0.006
Recall	0.430 ± 0.238	0.494 ± 0.018	0.519 ± 0.006	0.798 ± 0.029	$\mathbf{0.815 \pm 0.004}$
Mixed-hop Prediction (SNOMED-CT) : Average δ-hyperbolicity = 0.0255					
F1	0.129 ± 0.017	0.790 ± 0.012	0.672 ± 0.009	0.886 ± 0.027	$\mathbf{0.890 \pm 0.004}$
Precision	0.084 ± 0.001	0.950 ± 0.002	0.886 ± 0.003	0.894 ± 0.024	$\mathbf{0.901 \pm 0.006}$
Recall	0.375 ± 0.207	0.673 ± 0.019	0.541 ± 0.012	0.877 ± 0.032	$\mathbf{0.880 \pm 0.005}$
Multi-hop Inference (WordNet) : Average δ-hyperbolicity = 0.1431					
F1	0.134 ± 0.045	0.603 ± 0.009	0.648 ± 0.012	0.865 ± 0.026	$\mathbf{0.872 \pm 0.004}$
Precision	0.086 ± 0.016	0.739 ± 0.009	0.768 ± 0.012	0.867 ± 0.023	$\mathbf{0.871 \pm 0.007}$
Recall	0.431 ± 0.240	0.509 ± 0.011	0.560 ± 0.013	0.863 ± 0.031	$\mathbf{0.872 \pm 0.005}$
Multi-hop Inference (SNOMED-CT) : Average δ-hyperbolicity = 0.0254					
F1	0.128 ± 0.016	0.754 ± 0.025	0.630 ± 0.010	0.919 ± 0.028	$\mathbf{0.920 \pm 0.003}$
Precision	0.083 ± 0.001	0.969 ± 0.001	0.902 ± 0.002	0.917 ± 0.024	$\mathbf{0.919 \pm 0.008}$
Recall	0.369 ± 0.205	0.620 ± 0.031	0.483 ± 0.011	$\mathbf{0.921 \pm 0.034}$	0.920 ± 0.008

To validate our design choices, we conducted comprehensive ablation studies on loss components, pooling strategies, model depth, and negative sampling strategies which are presented in Appendix I.

5.2 Comparison with Hyperbolic Transformer Baseline

To further evaluate the effectiveness of HiM, we compare it with a hyperbolic transformer baseline. The original HiT (He et al., 2024b) fine-tunes a pretrained model (all-MiniLM-L6-v2, 22M params) with low curvature ($\mathcal{K} = -1/384$, nearly Euclidean). To isolate architectural effects and ensure fair comparison under identical training conditions, we implement HiT* using the MiniLM-L6-v2 transformer architecture trained from scratch (randomly initialized). We conducted ablations across two different curvatures ($\mathcal{K} = -1.0$ and $-1/d$ where embedding dimension $d = 384$) and model sizes (16M and 32M parameters) on both Poincaré and Lorentz manifolds. The results in Table 2 show that HiM consistently outperforms the transformer-

based HiT* model across both manifolds and most experimental configurations. See Appendix J for detailed model size configurations.

Table 2: F1 scores comparing HiM models with HiT* across different parameter scales and curvature settings on mixed-hop prediction tasks. HiT* (Hyperbolic Transformer with random initialization) uses identical hyperbolic projections, loss functions, and manifolds as HiM, differing only in the use of Transformer architecture instead of Mamba. Mean $\pm$ standard deviation computed over multiple independent runs. **Bold red** values indicate the best performance within each row, **bold blue** indicates second-best. Results demonstrate consistent advantages of the Mamba architecture over Transformers in hyperbolic settings.

#Param.	Curvature ($\mathcal{K}$)	Poincaré Manifold		Lorentz Manifold	
		HiM	HiT*	HiM	HiT*
WordNet Dataset					
16M	-1.0	$\textbf{\color{red}0.857 \pm 0.007}$	0.846 ± 0.006	$\textbf{\color{blue}0.851 \pm 0.004}$	0.838 ± 0.007
16M	$-1/d$	0.791 ± 0.012	$\textbf{\color{red}0.840 \pm 0.008}$	$\textbf{\color{blue}0.783 \pm 0.015}$	0.523 ± 0.025
32M	-1.0	$\textbf{\color{red}0.851 \pm 0.006}$	0.836 ± 0.007	$\textbf{\color{blue}0.839 \pm 0.005}$	0.829 ± 0.006
32M	$-1/d$	0.771 ± 0.011	$\textbf{\color{blue}0.809 \pm 0.014}$	$\textbf{\color{red}0.817 \pm 0.014}$	0.465 ± 0.030
DOID Dataset					
16M	-1.0	$\textbf{\color{red}0.904 \pm 0.008}$	0.837 ± 0.007	$\textbf{\color{blue}0.889 \pm 0.005}$	0.844 ± 0.005
16M	$-1/d$	$\textbf{\color{red}0.861 \pm 0.010}$	0.825 ± 0.009	$\textbf{\color{blue}0.706 \pm 0.018}$	0.518 ± 0.028
32M	-1.0	$\textbf{\color{red}0.881 \pm 0.007}$	0.831 ± 0.008	$\textbf{\color{blue}0.871 \pm 0.006}$	0.832 ± 0.007
32M	$-1/d$	$\textbf{\color{blue}0.837 \pm 0.009}$	0.835 ± 0.008	$\textbf{\color{red}0.709 \pm 0.016}$	0.527 ± 0.026

Notably, performance degrades significantly under low curvature settings ($\mathcal{K} = -1/d$), particularly in the Lorentz manifold, where HiT* shows substantial performance drops. This suggests that stronger hyperbolic curvature ($\mathcal{K} = -1.0$) is essential for effective hierarchical modeling. Under our fixed curvature, Poincaré's bounded nature enables more stable norm dispersion and discriminative gradient flow, particularly when combined with variance regularization in our centripetal loss. In contrast, Lorentz embeddings tend to collapse toward the hyperboloid's shell where time-like distances flatten and norm-based separation weakens. To provide broader context for our results, we include additional analysis with comparing our model to GPT-4o on zero-shot prompting as well as candidate ranking in Appendix H.2 and H.3 and also study HiM's computational efficiency in terms of sequence length in Appendix H.4. The success of hyperbolic embeddings in these tasks suggests broader potential for improving hierarchical reasoning in future generative models, where understanding semantic relationships could enhance factual consistency and knowledge grounding. Our results demonstrate that specialized embedding architectures can achieve strong performance on hierarchical reasoning tasks with significantly fewer parameters (16M) compared to general-purpose LLMs, offering a complementary approach to scaling.

5.3 Visualization of Hyperbolic Embeddings

To demonstrate how HiM captures hierarchical structure in the learned embeddings, we visualize the hyperbolic representations on a representative semantic hierarchy with WordNet. The hyperbolic embeddings learned by HiM is presented in Figure 2, which illustrates a representative hierarchical path, `sport` $\rightarrow$ `skating` $\rightarrow$ `skateboarding`. The HiM-trained embeddings exhibit tight clustering of semantically related nodes (e.g., `skating` and `sport`) in hyperbolic space, indicating enhanced semantic alignment. Moreover, the embeddings clearly capture the hierarchical structure, as higher-level concepts such as `sport` are positioned closer to the origin, while more specific concepts like `skateboarding` are embedded farther from the origin in a compact and organized manner. More details and geometric analysis of these hyperbolic embeddings, including quantitative metrics comparing h-norms, geodesic distances, and hierarchical depth correlations across both Poincaré and Lorentz manifolds, is provided in Appendix E. Additional examples from FoodOn dataset and out-of-distribution inference test are provided in Appendix G, along with the UMAP visualization methodology.
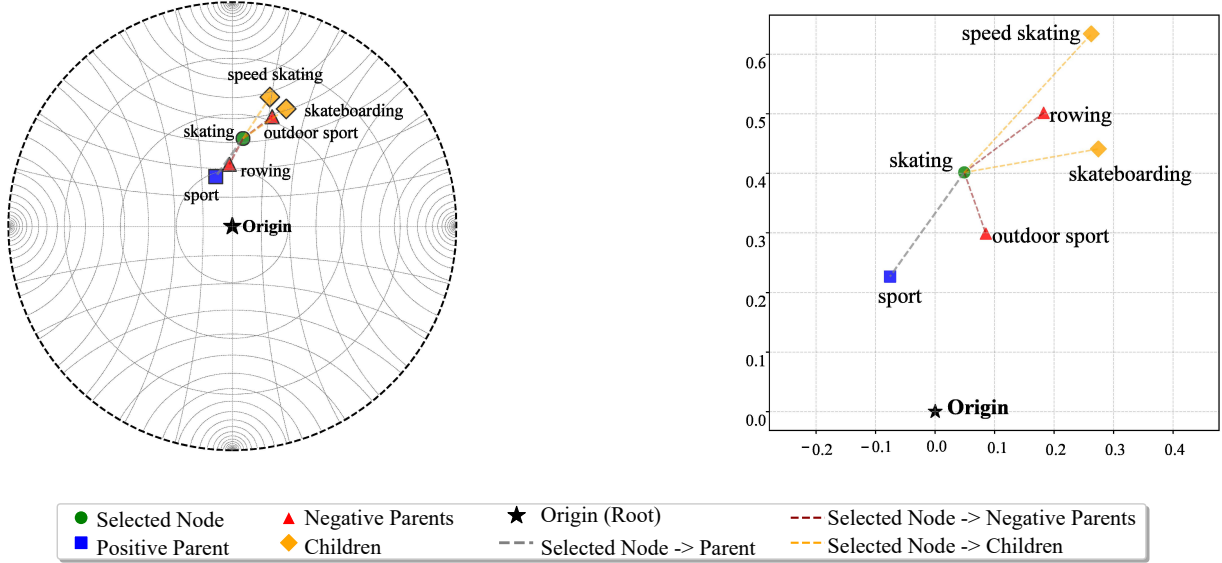
Figure 2: Visualization of HiM's embeddings trained on the WordNet dataset in the Poincaré ball manifold. **Left:** The full hyperbolic space, illustrating the distribution of entities with parent nodes positioned closer to the origin and child nodes extending toward the boundary, reflecting the exponential expansion of hyperbolic geometry. **Right:** A zoomed-in view emphasizing the hierarchical structure, such as the path sport → skating → skateboarding. Dots represent the entities, with colors indicating hierarchical relationships. For a selected node "skating" denoted by the green dot, the blue node denotes its parent nodes (e.g., sport), and red indicates its hard negatives, such as siblings/cousins (e.g., rowing). Yellow nodes (e.g, skateboarding, speed skating) indicate children nodes of the selected node (skating), meaning the grandchildren nodes of the blue node (sport).

6 Conclusion

By integrating hyperbolic embeddings in the model, HiM successfully captures hierarchical relationships in complex long-range datasets, providing a scalable and effective approach for handling long-range dependencies. HiM's unique approach, especially in hyperbolic embedding and its SSM incorporation, showcases its strengths in hierarchical long-range classification, marking it as a significant advancement in hierarchical learning models. Additionally, we find HiM to be more robust in training, primarily due to the Mamba2 blocks' efficient memory usage and the synergy between hyperbolic geometry and SSM-based sequence modeling.

Lorentz embeddings can provide a more natural fit for large-scale datasets with intricate hierarchical patterns compared to other geometries, potentially enhancing performance and interpretability. By demonstrating how a Lorentzian manifold can be effectively deployed for hyperbolic sentence representations, this paper aims to motivate further exploration of hyperbolic geometry in diverse real-world applications, ultimately broadening the scope and impact of geometry-aware neural architectures. Investigating HiM's potential for efficient temporal dependency modeling in intricate long-range hierarchical classification tasks holds significant promise and study its practical applications. Future work could explore integrating CLIP-style pretraining to incorporate multimodal data (e.g., text and images) for tasks like visual question answering, or potentially building on work such as Cobra (Zhao et al., 2025), which demonstrates the potential of extending Mamba models for efficient multimodal language modeling.

References

Aaron B. Adcock, Blair D. Sullivan, and Michael W. Mahoney. Tree-like structure in large social and information networks. In *2013 IEEE 13th International Conference on Data Mining*, pp. 1–10, 2013.

Gregorio Alanis-Lobato, Pablo Mier, and Miguel A Andrade-Navarro. Efficient embedding of complex networks to hyperbolic space via their laplacian. *Scientific reports*, 6(1):30108, 2016.

Cole Baker, Isabel Suárez-Méndez, Grace Smith, Elisabeth B Marsh, Michael Funke, John C Mosher, Fernando Maestú, Mengjia Xu, and Dimitrios Pantazis. Hyperbolic graph embedding of meg brain networks to study brain alterations in individuals with subjective cognitive decline. *IEEE Journal of Biomedical and Health Informatics*, 2024.

Samuel R Bowman, Gabor Angeli, Christopher Potts, and Christopher D Manning. The snli corpus. 2015.

Ines Chami, Zhitao Ying, Christopher Ré, and Jure Leskovec. Hyperbolic graph convolutional neural networks. *Advances in neural information processing systems*, 32, 2019.

Boli Chen, Yao Fu, Guangwei Xu, Pengjun Xie, Chuanqi Tan, Mosha Chen, and Liping Jing. Probing bert in hyperbolic spaces. In *International Conference on Learning Representations*, 2021.

Weize Chen, Xu Han, Yankai Lin, Kaichen He, Ruobing Xie, Jie Zhou, Zhiyuan Liu, and Maosong Sun. Hyperbolic pre-trained language model. *IEEE/ACM Transactions on Audio, Speech, and Language Processing*, 2024.

Noam Chomsky. Aspects of the theory of syntax. 1965.

Tri Dao and Albert Gu. Transformers are ssms: Generalized models and efficient algorithms through structured state space duality. *arXiv preprint arXiv:2405.21060*, 2024.

Jacob Devlin, Ming-Wei Chang, Kenton Lee, and Kristina Toutanova. Bert: Pre-training of deep bidirectional transformers for language understanding. In *Proceedings of the 2019 conference of the North American chapter of the association for computational linguistics: human language technologies, volume 1 (long and short papers)*, pp. 4171–4186, 2019.

Bhuwan Dhingra, Christopher J Shallue, Mohammad Norouzi, Andrew M Dai, and George E Dahl. Embedding text in hyperbolic spaces. *arXiv preprint arXiv:1806.04313*, 2018.

Damion M Dooley, Emma J Griffiths, Gurinder S Gosal, Pier L Buttigieg, Robert Hoehndorf, Matthew C Lange, Lynn M Schriml, Fiona SL Brinkman, and William WL Hsiao. Foodon: a harmonized food ontology to increase global food traceability, quality control and data integration. *npj Science of Food*, 2(1):23, 2018.

Xiran Fan, Minghua Xu, Huiyuan Chen, Yuzhong Chen, Mahashweta Das, and Hao Yang. Enhancing hyperbolic knowledge graph embeddings via lorentz transformations. In *Findings of the Association for Computational Linguistics ACL 2024*, pp. 4575–4589, 2024.

Octavian Ganea, Gary Bécigneul, and Thomas Hofmann. Hyperbolic entailment cones for learning hierarchical embeddings. In *International conference on machine learning*, pp. 1646–1655. PMLR, 2018.

Mikhael Gromov. Hyperbolic groups. In *Essays in group theory*, pp. 75–263. Springer, 1987.

Albert Gu and Tri Dao. Mamba: Linear-time sequence modeling with selective state spaces. *arXiv preprint arXiv:2312.00752*, 2023.

Albert Gu, Karan Goel, and Christopher Ré. Efficiently modeling long sequences with structured state spaces. *arXiv preprint arXiv:2111.00396*, 2021.

Yuan He, Jiaoyan Chen, Hang Dong, Ian Horrocks, Carlo Allocca, Taehun Kim, and Brahmananda Sapkota. Deeponto: A python package for ontology engineering with deep learning. *Semantic Web*, 15(5):1991–2004, 2024a.

Yuan He, Moy Yuan, Jiaoyan Chen, and Ian Horrocks. Language models as hierarchy encoders. *Advances in Neural Information Processing Systems*, 37:14690–14711, 2024b.

Edward J Hu, Yelong Shen, Phillip Wallis, Zeyuan Allen-Zhu, Yuanzhi Li, Shean Wang, Lu Wang, Weizhu Chen, et al. Lora: Low-rank adaptation of large language models. *ICLR*, 1(2):3, 2022.

John D Hunter. Matplotlib: A 2d graphics environment. *Computing in science & engineering*, 9(03):90–95, 2007.

Max Kochurov, Rasul Karimov, and Serge Kozlukov. Geoopt: Riemannian optimization in pytorch. *arXiv preprint arXiv:2005.02819*, 2020.

Dmitri Krioukov, Fragkiskos Papadopoulos, Maksim Kitsak, Amin Vahdat, and Marián Boguná. Hyperbolic geometry of complex networks. *Physical Review E—Statistical, Nonlinear, and Soft Matter Physics*, 82 (3):036106, 2010.

Qiuyu Liang, Weihua Wang, Feilong Bao, and Guanglai Gao. Lˆ 2gc: Lorentzian linear graph convolutional networks for node classification. *arXiv preprint arXiv:2403.06064*, 2024.

Qi Liu, Maximilian Nickel, and Douwe Kiela. Hyperbolic graph neural networks. *Advances in neural information processing systems*, 32, 2019.

Federico López and Michael Strube. A fully hyperbolic neural model for hierarchical multi-class classification. In *Findings of the Association for Computational Linguistics: EMNLP 2020*. Association for Computational Linguistics, November 2020.

Paolo Mandica, Luca Franco, Konstantinos Kallidromitis, Suzanne Petryk, and Fabio Galasso. Hyperbolic learning with multimodal large language models. *arXiv preprint arXiv:2408.05097*, 2024.

Leland McInnes, John Healy, and James Melville. Umap: Uniform manifold approximation and projection for dimension reduction. *arXiv preprint arXiv:1802.03426*, 2018.

George Miller. Wordnet: a lexical database for english communications of the acm 38 (11) 3941. *Niemela, I*, 1995.

Gal Mishne, Zhengchao Wan, Yusu Wang, and Sheng Yang. The numerical stability of hyperbolic representation learning. In *Proceedings of the 40th International Conference on Machine Learning*, Proceedings of Machine Learning Research, pp. 24925–24949. PMLR, 2023.

Maximillian Nickel and Douwe Kiela. Poincaré embeddings for learning hierarchical representations. *Advances in neural information processing systems*, 30, 2017.

Maximillian Nickel and Douwe Kiela. Learning continuous hierarchies in the lorentz model of hyperbolic geometry. In *International conference on machine learning*, pp. 3779–3788. PMLR, 2018.

A Paszke. Pytorch: An imperative style, high-performance deep learning library. *arXiv preprint arXiv:1912.01703*, 2019.

Wei Peng, Tuomas Varanka, Abdelrahman Mostafa, Henglin Shi, and Guoying Zhao. Hyperbolic deep neural networks: A survey. *IEEE Transactions on pattern analysis and machine intelligence*, 44(12):10023–10044, 2021.

Igor Petrovski. Hyperbolic sentence representations for solving textual entailment. *arXiv preprint arXiv:2406.15472*, 2024.

Hugo Ramirez, Davide Tabarelli, Arianna Brancaccio, Paolo Belardinelli, Elisabeth B Marsh, Michael Funke, John C Mosher, Fernando Maestu, Mengjia Xu, and Dimitrios Pantazis. Fully hyperbolic neural networks: A novel approach to studying aging trajectories. *IEEE Journal of Biomedical and Health Informatics*, 2025.

Lynn Marie Schriml, Cesar Arze, Suvarna Nadendla, Yu-Wei Wayne Chang, Mark Mazaitis, Victor Felix, Gang Feng, and Warren Alden Kibbe. Disease ontology: a backbone for disease semantic integration. *Nucleic acids research*, 40(D1):D940–D946, 2012.

Florian Schroff, Dmitry Kalenichenko, and James Philbin. Facenet: A unified embedding for face recognition and clustering. In *Proceedings of the IEEE conference on computer vision and pattern recognition*, pp. 815–823, 2015.

Michael Q Stearns, Colin Price, Kent A Spackman, and Amy Y Wang. Snomed clinical terms: overview of the development process and project status. In *Proceedings of the AMIA Symposium*, pp. 662, 2001.

Alexandru Tifrea, Gary Bécigneul, and Octavian-Eugen Ganea. Poincaré glove: Hyperbolic word embeddings. *arXiv preprint arXiv:1810.06546*, 2018.

Ashish Vaswani, Noam Shazeer, Niki Parmar, Jakob Uszkoreit, Llion Jones, Aidan N Gomez, Łukasz Kaiser, and Illia Polosukhin. Attention is all you need. *Advances in neural information processing systems*, 30, 2017.

Menglin Yang, Aosong Feng, Bo Xiong, Jiahong Liu, Irwin King, and Rex Ying. Enhancing llm complex reasoning capability through hyperbolic geometry. In *ICML 2024 Workshop on LLMs and Cognition*, 2024a.

Menglin Yang, Aosong Feng, Bo Xiong, Jihong Liu, Irwin King, and Rex Ying. Hyperbolic fine-tuning for large language models. *arXiv preprint arXiv:2410.04010*, 2024b.

Zhe Yang, Wenrui Li, and Guanghui Cheng. SHMamba: Structured hyperbolic state space model for audio-visual question answering. *arXiv preprint arXiv:2406.09833*, 2024c.

Han Zhao, Min Zhang, Wei Zhao, Pengxiang Ding, Siteng Huang, and Donglin Wang. Cobra: Extending mamba to multi-modal large language model for efficient inference. In *Proceedings of the AAAI Conference on Artificial Intelligence*, volume 39, pp. 10421–10429, 2025.

A Preliminaries

A.1 Hyperbolic Geometry

In hyperbolic geometry, the notion of curvature is commonly represented by negative curvature $\mathcal{K} = -\frac{1}{c}$, where $c > 0$. Equivalently, one may define a 'radius' $r = \sqrt{c}$. A smaller radius r corresponds to a larger and higher negative curvature ($\mathcal{K}$), effectively making the hyperbolic manifold more curved, granting more flexibility to the hierarchical depth. Conversely, letting $r \to \infty$ approaches flat (Euclidean) space since $\mathcal{K} \to 0$. Basically, r controls the rate of exponential expansion on the hyperbolic manifold. This choice impacts how data at varying levels of abstraction distributes on the manifold and is crucial for tasks requiring fine-grained or exponential separation of hierarchical data. By leveraging hyperbolic space, language models can encode features more naturally in a hierarchical branching, keeping more generalized features located near the root of the hierarchy tree, i.e., near the origin of the Hyperbolic Manifold, and the more specific or complex entities are branched further from the origin towards the margin.

A popular way to realize hyperbolic geometry in an n-dimensional setting is via the Poincaré ball model. Here, the underlying space is the open Poincaré unit ball:

$$\mathcal{B}^n = \{\mathbf{x} \in \mathbb{R}^n : \|\mathbf{x}\| < \sqrt{c}\}, \tag{11}$$

equipped with a metric tensor that expands distances near the boundary. Concretely, each point $\mathbf{x}$ in the ball maintains a local geometry that grows increasingly "stretched" as $\|\mathbf{x}\|$ approaches radius $\sqrt{c}$. Formally, the distance between two points $\mathbf{x}$ and $\mathbf{y}$ in a Poincaré ball is computed by

$$d_{\mathcal{P}}(\mathbf{x}, \mathbf{y}) = \sqrt{c} \cdot \text{arcosh}\left(1 + 2\frac{\|\mathbf{x} - \mathbf{y}\|^2}{(1 - \|\mathbf{x}\|^2/c)(1 - \|\mathbf{y}\|^2/c)}\right). \tag{12}$$

This representation has gained attention in machine learning due to relatively simple re-parameterizations for gradient-based updates, thus facilitating the embedding of hierarchically structured data (Nickel & Kiela, 2017).

While the Poincaré ball confines all points within the unit sphere (Equation 11), the Lorentzian manifold leverages an $(n + 1)$-dimensional Minkowski space (Equation 13), enabling a different perspective on hyperbolic geometry. Specifically, points reside on the "hyperboloid" defined by:

$$\mathcal{L}^n = \{\mathbf{x} \in \mathbb{R}^{n+1} : \langle \mathbf{x}, \mathbf{x} \rangle_M = -c, \ x_0 > 0\}, \tag{13}$$

where $\langle \cdot, \cdot \rangle_M$ denotes the Minkowski inner product, typically $-x_0 y_0 + \sum_{i=1}^{n} x_i y_i$. The hyperbolic distance between two points $\mathbf{x}$ and $\mathbf{y}$ then appears in the form:

$$d_{\mathcal{L}}(\mathbf{x}, \mathbf{y}) = \sqrt{c} \cdot \operatorname{arcosh}\left(-\frac{\langle \mathbf{x}, \mathbf{y} \rangle_M}{c}\right). \tag{14}$$

Compared to the Poincaré ball, this approach can sidestep certain numerical instabilities near the boundary because vectors are not constrained to lie within a finite radius. Moreover, Lorentz-based formulations often allow more direct computation of geodesics and exponential maps, making them advantageous for large-scale hyperbolic embeddings (Nickel & Kiela, 2018). Krioukov et al. (2010) provides a theoretical foundation for the hyperbolic geometry of complex networks, showing that many real-world networks naturally embed into hyperbolic spaces, supporting our choice of the Poincaré and Lorentzian models for hierarchical language embeddings.
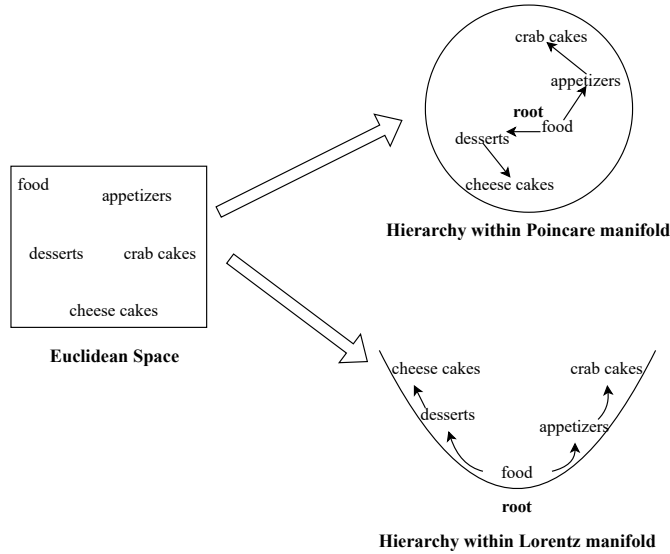

Figure 3: Illustration of word embeddings in Euclidean (Left) vs. Hyperbolic Spaces for hierarchical representation in Poincaré (Top right) and Lorentzian Manifolds (Bottom right).

We can see how hierarchies are represented differently in Euclidean space, the Poincaré manifold, and the Lorentzian manifold as illustrated in Figure 3. On the left, the hierarchical structure is arranged as a standard tree. While the relationships are maintained, Euclidean space does not naturally encode hierarchical distances in 2D. In Figure 3 the upper-right diagram shows the hierarchy embedded into the Poincaré ball (the root/origin being at the center). The more generalized parent nodes are positioned near origin, and descendant nodes extend outward near the margin. This representation captures the exponential growth of hierarchical structures, where sibling nodes are placed far apart in terms of geodesic distance. The lower-right diagram visualizes the same hierarchy embedded in the Lorentz hyperboloid. The Lorentzian manifold in $\mathbb{R}^{n+1}$ consists of n spatial dimensions and one time-like dimension (x_0). The origin is at the center-bottom of the Hyperboloid, and nodes are arranged along the hyperboloid surface. More generalized parent nodes are positioned near the bottom, and the descendants keep extending upward on the cone of Lorentz. Unlike the Poincaré model, which confines embeddings within a finite ball, the Lorentz model represents hierarchies in an unbounded space, making it particularly suitable for representing deeply nested hierarchies.

A.2 Mamba2

Mamba2 is a state-space model (SSM) introduced by Tri Dao and Albert Gu that refines the original Mamba architecture with improved performance and simplified design (Dao & Gu, 2024). Mamba-2 builds

upon the original Mamba architecture by introducing the State Space Duality (SSD) framework, which establishes theoretical connections between State Space Models (SSMs) and attention mechanisms. Mamba2 achieves 2-8× faster processing while maintaining competitive performance compared to Transformers for language modeling tasks. In order to formulate the overall computation for a single Mamba2 block, let $\mathbf{x}_{1:L} = [\mathbf{x}_1, \ldots, \mathbf{x}_L]$ be the token (or embedding) sequence for a given input. A single Mamba2 block transforms $\mathbf{x}_{1:L}$ into an output sequence $\mathbf{y}_{1:L}$. Each input token embedding $\mathbf{x}_t \in \mathbb{R}^D$ is first normalized via RMSNorm. RMS normalization ensures that the norm of the embeddings remains stable across different inputs, preventing extreme values from causing instability during training.

$$\widetilde{\mathbf{x}}_t = \text{RMSNorm}(\mathbf{x}_t). \tag{15}$$

Given weights W and bias b, we project the input into a higher-dimensional space to obtain $\mathbf{u}$.

$$\mathbf{u}_t = W_{\text{in}}\,\widetilde{\mathbf{x}}_t + \mathbf{b}_{\text{in}}, \tag{16}$$

yielding $\mathbf{u}_t \in \mathbb{R}^I$. $\mathbf{u}_t$ is split it into two components, $\mathbf{x}'_t$ and $\mathbf{z}'_t$.

$$\mathbf{u_t} = \begin{bmatrix} \mathbf{x}'_t \\ \mathbf{z}'_t \end{bmatrix}. \tag{17}$$

The component $\mathbf{z}'_t$ is reserved for the gating mechanism used later in the process. For each time step t, hidden states $\mathbf{h}_t$ evolve under:

$$\mathbf{h}_t = \mathbf{A}_t \mathbf{h}_{t-1} + \mathbf{B}_t \mathbf{x}_t, \quad \mathbf{y}_t = \mathbf{C}_t \mathbf{h}_t \tag{18}$$

where $\mathbf{A}_t$ is the state transition matrix, $\mathbf{B}_t$ is the input projection, and $\mathbf{C}_t$ is the output projection.

For each timestep t, the state matrices have dimensions $\mathbf{A}_t \in \mathbb{R}^{N \times N}$, $\mathbf{B}_t \in \mathbb{R}^{N \times I}$, and $\mathbf{C}_t \in \mathbb{R}^{I \times N}$, where N is the state dimension and I is the intermediate dimension. To enable efficient $O(L)$ complexity, Mamba2 uses *structured* versions of A, B, C (e.g., diagonal-plus-low-rank forms) and fast transforms (such as FFT-based convolution). Mamba2 incorporates a gating mechanism to blend the output of the state-space layer back with the original input, thus forming a residual block:

$$\mathbf{y}_t = \sigma(\mathbf{g}_t)\,\mathbf{z}_t + \mathbf{x}_t, \quad \mathbf{g}_t = W_g\,\widetilde{\mathbf{x}}_t + \mathbf{b}_g, \tag{19}$$

where $\sigma(\cdot)$ is typically a SiLU activation that follows this operation for non-linearity.

$$\sigma(x) = x \cdot sigmoid(x), \quad sigmoid(x) = \frac{1}{1 + e^{-x}}. \tag{20}$$

This gating helps regulate the flow of information and provides additional stability during training.

Mamba2 establishes a theoretical framework connecting SSMs and attention mechanisms through "state space duality", allowing the model to function either as an SSM or as a structured form of attention via the below formulation:

$$\mathcal{L} := 1\text{SS}(a) \quad \text{and} \quad M = \mathcal{L} \circ \left(C\,B^\top \right). \tag{21}$$

where $\mathcal{L}$ is the semiseparable matrix structure derived from the state transition dynamics, $\circ$ denotes the Hadamard (element-wise) product. Following Dao & Gu (2024), we denote a *1-semiseparable (1-SS) matrix* generated by scalar sequence $a = (a_0, a_1, \ldots, a_{L-1})$ as $1\text{SS}(a)$. This is a lower-triangular matrix $\mathcal{L} \in \mathbb{R}^{L \times L}$ where:

$$\mathcal{L}_{i,i} = 1, \quad \mathcal{L}_{i,j} = \prod_{k=j+1}^{i} a_k \quad \text{for } i > j \tag{22}$$

This structure enables efficient $\mathcal{O}(L)$ computation via parallel scan operations, which is fundamental to Mamba2's hardware-efficient implementation. This paper introduces a Mamba2-based LLM known as SentenceMamba-16M, a lightweight model with 16M parameters, suitable for resource-efficient and high-quality sentence embedding generation. As we can see in Figure 1, we incorporate four Mamba2 blocks in our SentenceMamba-16M for efficient state-space modeling.

B Hyperbolic Loss Calculations

Depending on our dataset, we can either apply Triplet Loss when we have a triplet relationship in our data and need to enforce relative distance constraints or apply Contrastive Loss when we have pairwise relationships in our data and need to classify pairs as similar or dissimilar. Based on either triplet relationship data or pairwise relationship data, we perform triplet loss or contrastive loss calculation. Then, we calculate the weighted loss of centripetal loss and clustering loss as the hyperbolic loss. Hyperbolic loss computation framework is illustrated in Figure 4, which shows how these two loss components are weighted and combined to create the final training objective. Loss minimization involves clustering related entities and distancing unrelated ones (clustering loss) and tightening parent entities closer to the hyperbolic manifold's origin than their child counterparts (centripetal loss), giving it a hierarchical structure.
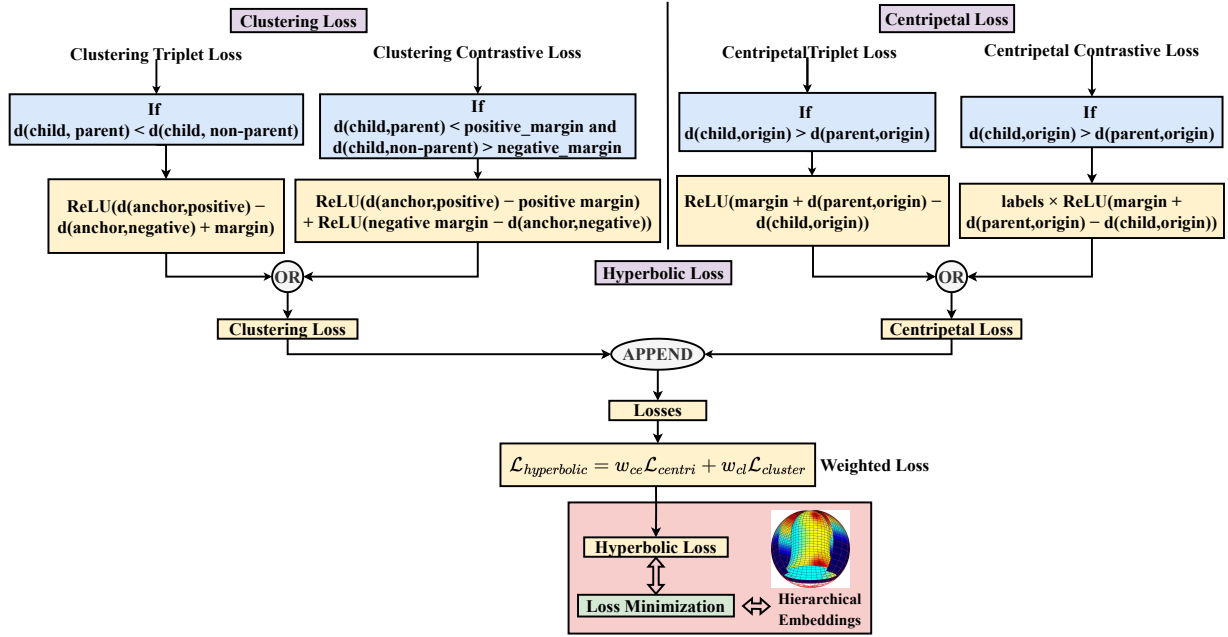

Figure 4: Calculation of hyperbolic loss from clustering loss and centripetal loss.

C Dataset Statistics

To provide a comprehensive overview of the datasets used in our experiments, we detail the size, number of entities (nodes), and train/validation/test splits for each dataset in Table 3. These datasets are represented as directed acyclic graphs (DAGs), where nodes denote entities (e.g., diseases in DOID, synsets in WordNet) and edges denote direct subsumption relations (is-a). Splits are created by sampling direct (E) and indirect (multi-hop, T) subsumptions, ensuring coverage of both mixed-hop prediction and multi-hop inference tasks.

Table 3: Statistics of hierarchical ontology datasets

Dataset	#Entities	#DirectSub	#IndirectSub	Splits (Train/Val/Test)
DOID	11,157	11,180	45,383	Mixed-hop: 111K / 31K / 31K
FoodOn	30,963	36,486	438,266	Mixed-hop: 361K / 261K / 261K
WordNet (Noun)	74,401	75,850	587,658	Multi-hop: 834K / 323K / 323K
				Mixed-hop: 751K / 365K / 365K
SNOMED-CT	364,352	420,193	2,775,696	Multi-hop: 4,160K /1,758K/1,758K
				Mixed-hop: 4,160K/1,758K/1,758K

D Task Formulations

D.1 Multi-Hop inference

Let $G = (V, E)$ denote a hierarchical graph, where V represents entities (nodes) and E denotes direct subsumption edges (e.g., parent-child relationships). The transitive closure T of E encompasses all indirect (multi-hop) subsumptions, such as relationships spanning two or more hops (e.g., grandparent-to-grandchild). The multi-hop inference task trains a model f_{MI} on the direct edges E and evaluates its ability to predict the existence of unseen indirect relations in T:

$$f_{\mathrm{MI}} : (V, E) \rightarrow \hat{T}, \tag{23}$$

where $\hat{T}$ approximates T. This binary classification task tests transitive reasoning, such as inferring "dog is a vertebrate" from "dog is a mammal" and "mammal is a vertebrate." The model computes hyperbolic distances between entity embeddings, with a threshold determining relationship existence.

Evaluation uses precision, recall, and $F1_{\mathrm{MI}}$ scores over test pairs sampled from $T \cup N$, where N represents negative pairs (non-subsumptions). Test sets S_{test} are constructed as:

$$S_{\mathrm{test}} = \{(v_i, v_j) \mid (v_i, v_j) \in T \cup N, |N| = 10|T|\}, \tag{24}$$

with negatives, including hard cases like sibling entities (sharing a parent but not directly or transitively linked). This assesses fine-grained discrimination across both upward (child-to-ancestor) and downward (parent-to-descendant) directions, leveraging HiM's hyperbolic embeddings.

D.2 Mixed-Hop prediction

The mixed-hop prediction task evaluates the model's ability to predict the exact number of hops between entities, encompassing both direct (1-hop) and multi-hop (2+ hops) subsumptions. Given a training subset E, the model f_{MP} is trained and tested on:

$$f_{\mathrm{MP}} : (V, E) \rightarrow \hat{R}, \tag{25}$$

where $R = E \cup T$ includes all held-out direct and transitive subsumptions, and $\hat{R}$ approximates R. Unlike multi-hop inference, which focuses on existence, mixed-hop prediction quantifies hierarchical distance (e.g., 1, 2, or 3 hops), such as distinguishing "dog to mammal" (1 hop) from "dog to vertebrate" (2 hops). This is framed as a multi-class classification task, mapping hyperbolic distances to discrete hop counts.

Evaluation employs $F1_{\mathrm{MP}}$ scores over test sets:

$$S_{\mathrm{test}} = \{(v_i, v_j) \mid (v_i, v_j) \in (E \cup T) \cup N, |N| = 10|E \cup T|\}, \tag{26}$$

where positive pairs from $E \cup T$ are labeled with their true hop distances, and negatives (e.g., siblings or unrelated entities) are included at a 1:10 ratio. Hard negatives, such as sibling pairs sharing a parent v_k without a subsumption link, enhance the task's difficulty. This bidirectional task also assesses reasoning in both upward and downward directions.

E Learning Interpretable Hierarchical Semantics Through Hyperbolic Geometry

To provide more interpretable results of our HiM models for the hierarchical learning, we conducted a deeper geometric analysis of the hyperbolic entity embeddings for semantically related WordNet entities under **HiM-Poincaré** and **HiM-Lorentz** manifolds (see the visualization of hyperbolic embeddings in Figure 2). Specifically, we computed three key metrics with the learned hyperbolic embeddings: 1) "**hyperbolic geodesic distances**" between each pair of entities, 2) "**h-norm**" represents the norm distance from the origin, a higher h-norm often indicates a deeper or more specific concept in the hierarchy, 3) "**depth**" is the WordNet tree depth. In both sets of entities, the h-norm correlates strongly with the hierarchical depth, see Figure 5. For instance, in Table 4, the entity `sport` (depth 9) has an h-norm of 0.55, while `skateboarding`

17

(depth 12) has an h-norm of 2.25, reflecting the hierarchical expansion from general to specific concepts. However, a key difference emerges when comparing the two manifolds: **HiM-Lorentz** consistently produces smaller hyperbolic distances and h-norms compared to **HiM-Poincaré**. For example, in Table 5 (HiM-Lorentz), the parent-child relationships (e.g., *sport → skating → skateboarding*) have tighter distances and h-norm gradients compared to Table 4.
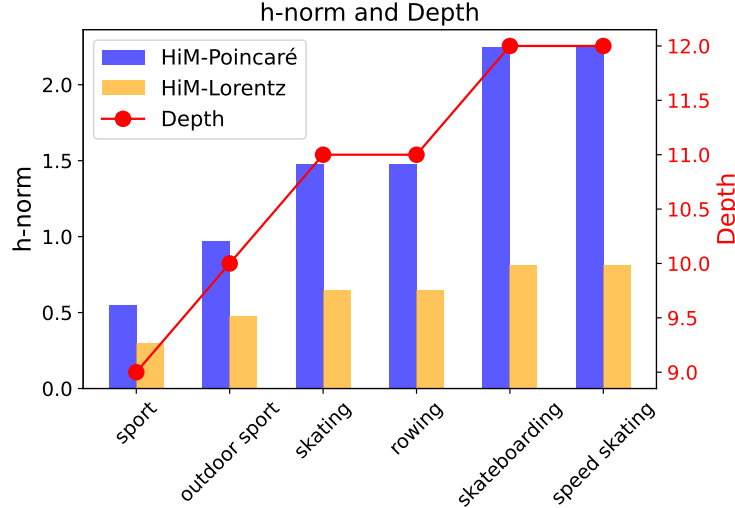

Figure 5: Alignment between the computed h-norms (derived from hyperbolic embeddings by HiM-Poinaré and HiM-Lorentz) and the actual tree-depth for sports-related entities in the WordNet dataset. As the depth increases from general terms like "sport" to specific ones like "skateboarding" and "speed skating", both HiM models show increasing h-norms, reflecting the underlying hierarchical structure. While *HiM-Poincaré produces higher h-norms that better differentiate fine-grained semantic levels*, while *HiM-Lorentz yields more compact yet hierarchy-preserving embeddings with improved numerical stability*. Our results illustrate that both HiM models effectively encode semantic hierarchy, with **Poincaré favoring detail and Lorentz emphasizing robustness**.

This reduction in distances under the Lorentz manifold is advantageous for hierarchical modeling. The Lorentz model's unbounded nature avoids the boundary constraints of the Poincaré ball, which can lead to numerical instability near the boundary. By mapping embeddings into an unbounded hyperboloid, **HiM-Lorentz** achieves tighter clustering of related entities (e.g., between `sport` and `skating`: 0.73 h-Norm of HiM-Lorentz vs. 1.67 h-norm of HiM-Poincaré) while maintaining the hierarchical structure. This tighter clustering enhances the model's ability to distinguish fine-grained relationships, especially in deeper hierarchies, as evidenced by the smaller standard deviations of **HiM-Lorentz** in performance metrics (Table 1).

F   Performance Comparisons between Hyperbolic embeddings and Euclidean embeddings

For `mixed-hop prediction` (Figure 6), **HiM-Lorentz** achieves better performance on datasets with deeper hierarchies, such as DOID (δ-hyperbolicity = 0.019) and SNOMED-CT (δ-hyperbolicity = 0.026). This aligns with the Lorentz manifold's ability to handle deeply nested structures more effectively. However, for FoodOn (δ-hyperbolicity = 0.185), **HiM-Poincaré** slightly outperforms **HiM-Lorentz**. FoodOn's higher δ-hyperbolicity indicates a less tree-like structure, suggesting that the Poincaré model's bounded nature may better capture less hierarchical relationships in certain contexts. Both hyperbolic models significantly outperform the Euclidean baselines.

Table 4: Hyperbolic distances, h-norms, and depths for sports-related entities (from Figure 2) using **HiM-Poincaré**, sorted by increasing depth.

	sport	outdoor sport	skating	rowing	skateboarding	speed skating
sport	0.00	1.17	1.67	1.62	2.43	2.40
outdoor sport	1.17	0.00	1.90	1.95	2.66	2.62
skating	1.67	1.90	0.00	2.36	3.12	3.07
rowing	1.62	1.95	2.36	0.00	3.10	3.11
skateboarding	2.43	2.66	3.12	3.10	0.00	3.76
speed skating	2.40	2.62	3.07	3.11	3.76	0.00
h-norm	0.55	0.97	1.48	1.48	2.25	2.25
depth	9	10	11	11	12	12

Table 5: Hyperbolic distances, h-norms, and depths for sports-related entities (from Figure 2) using **HiM-Lorentz**, sorted by increasing depth.

	sport	outdoor sport	skating	rowing	skateboarding	speed skating
sport	0.00	0.55	0.73	0.71	0.87	0.87
outdoor sport	0.55	0.00	0.79	0.87	0.98	0.95
skating	0.73	0.79	0.00	0.95	1.08	1.08
rowing	0.71	0.87	0.95	0.00	1.07	1.07
skateboarding	0.87	0.98	1.08	1.07	0.00	1.20
speed skating	0.87	0.95	1.08	1.07	1.20	0.00
h-norm	0.30	0.48	0.65	0.65	0.81	0.81
depth	9	10	11	11	12	12

In `multi-hop inference` (Figure 7), **HiM-Lorentz** again demonstrates robust performance, particularly on SNOMED-CT and WordNet, which exhibit deeper hierarchies (SNOMED-CT δ-hyperbolicity = 0.0254, WordNet δ-hyperbolicity = 0.1431). The smaller standard deviations in **HiM-Lorentz**'s metrics (e.g., 0.003 for SNOMED-CT F1) compared to **HiM-Poincaré** (0.028) highlight its stability, a benefit of the Lorentz manifold's numerical advantages. Notably, **HiM-Poincaré** achieves a slightly higher recall on SNOMED-CT, suggesting that the bounded nature of the Poincaré ball can occasionally enhance sensitivity. However, the overall F1 score favors **HiM-Lorentz**, indicating better balance in precision and recall.

A key observation across both tasks is the impact of dataset's tree-like structure as measured by δ-hyperbolicity. Datasets with lower δ-hyperbolicity (meaning more tree-like) benefit more from **HiM-Lorentz**, as its unbounded manifold better captures the exponential expansion of deep hierarchies. In contrast, FoodOn's higher δ-hyperbolicity correlates with **HiM-Poincaré**'s better performance, suggesting that the choice of manifold may depend on the dataset's structural properties.

Figures 8 to 10 illustrate the training dynamics of HiM-Poincaré and HiM-Lorentz across epochs for each dataset and task, plotting Hyperbolic Loss and F1 Score. The Hyperbolic Loss decreases steadily for both models across all datasets, indicating effective optimization of hierarchical relationships. HiM-Lorentz often exhibits a slightly faster convergence rate and lower final loss compared to HiM-Poincaré, reflecting the Lorentz manifold's suitability for capturing exponential hierarchical expansion. The F1 Score trends mirror the loss behavior, with HiM-Lorentz often achieving slightly better F1 scores.
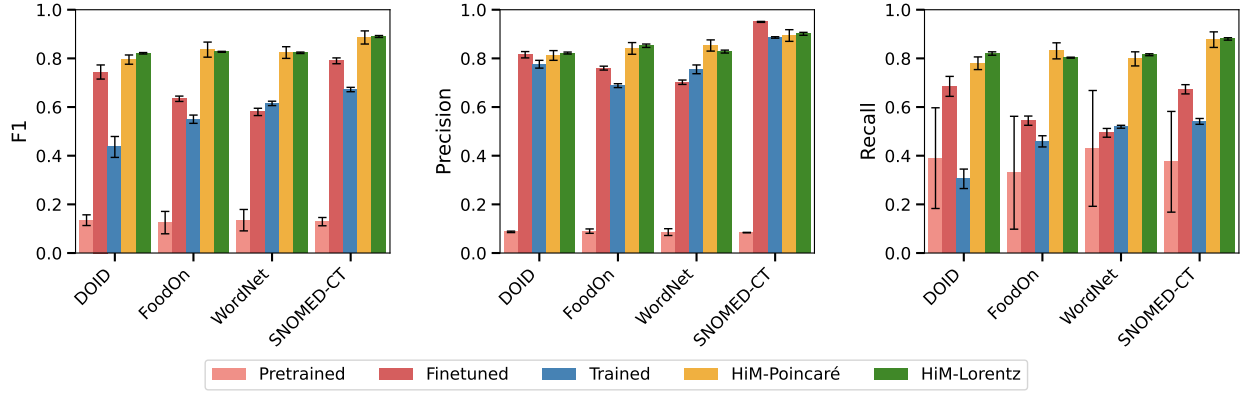
Figure 6: Comparisons of `mixed-hop prediction` performance for DOID, FoodOn, WordNet, and SNOMED-CT datasets across our proposed hyperbolic Mamba (HiM) models–*HiM-Poincaré* and *HiM-Lorentz*–and their Euclidean counterparts: *Pretrained, Finetuned (with pretrained weights)*, and *Trained from scratch* SentenceMamba-16M. HiM models trained from scratch in hyperbolic space substantially outperform all Euclidean baselines including the finetuned variant.
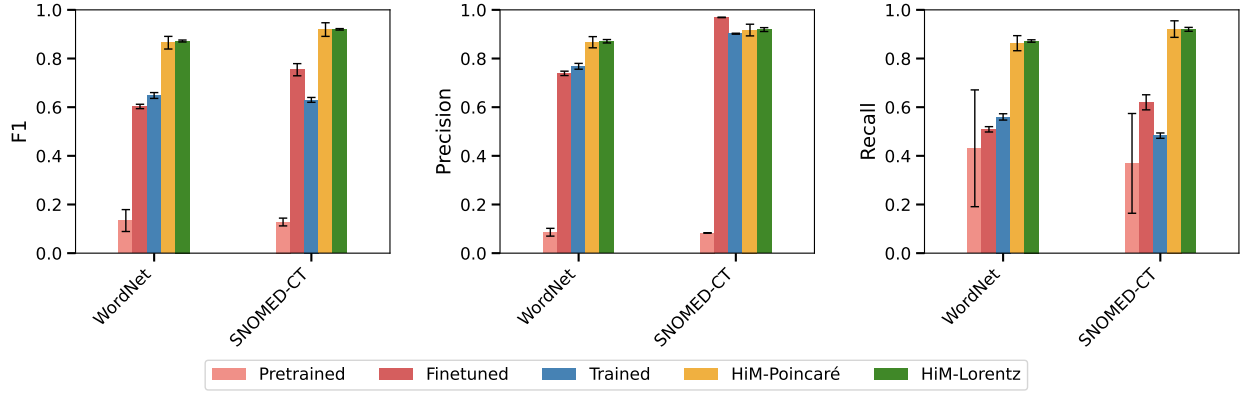

Figure 7: Comparisons of `multi-hop inference` performance for WordNet and SNOMED-CT datasets across our proposed hyperbolic Mamba (HiM) models–*HiM-Poincaré* and *HiM-Lorentz*–and their Euclidean counterparts: *Pretrained, Finetuned (with pretrained weights)*, and *Trained from scratch* SentenceMamba-16M. Hyperbolic models demonstrate superior hierarchical reasoning capabilities compared to all Euclidean variants.
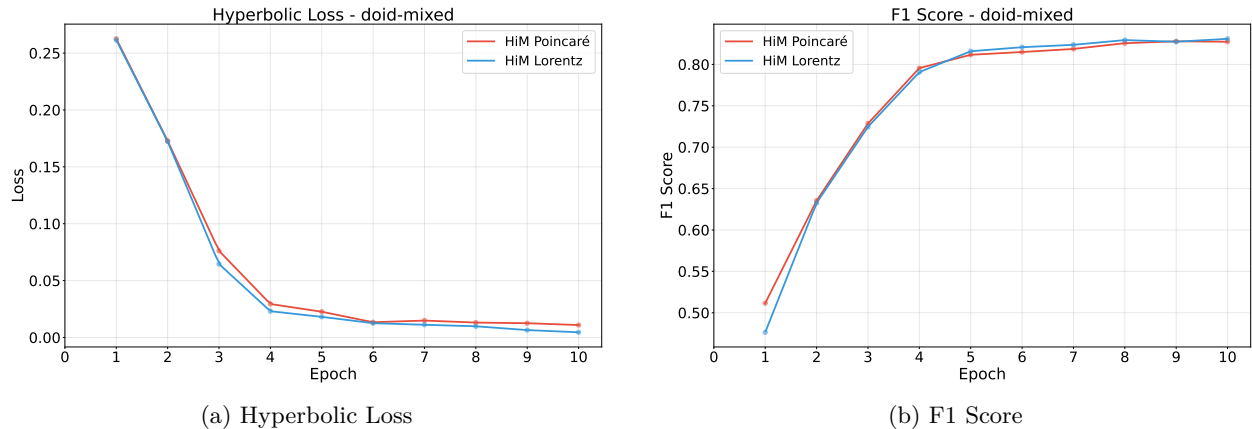

(a) Hyperbolic Loss

(b) F1 Score

Figure 8: Comparison of hyperbolic loss and F1 score on **DOID mixed-hop prediction** across epochs.
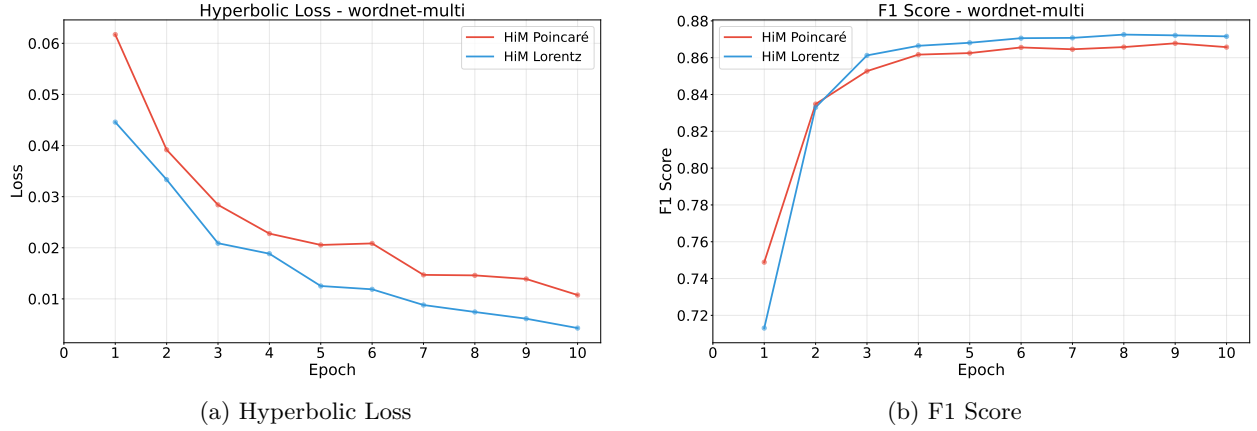
(a) Hyperbolic Loss

(b) F1 Score

Figure 9: Comparison of hyperbolic loss and F1 score on **WordNet multi-hop inference** across epochs.

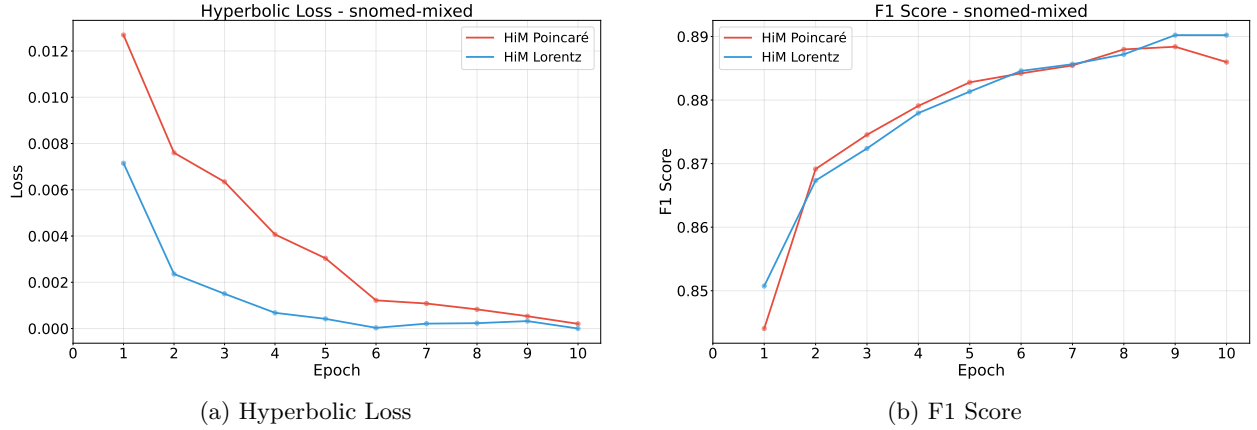(a) Hyperbolic Loss

(b) F1 Score

Figure 10: Comparison of hyperbolic loss and F1 score on **SNOMED-CT mixed-hop prediction** across the epochs.

G   Additional Hierarchical Embedding Visualizations

G.1   FoodOn Ontology: Fruit Hierarchy

Figure 11 shows HiM's learned embeddings for the FoodOn hierarchy `fruit`→`nut fruit`→`{filbert nut, common hazelnut}`.

HiM Trained (Left): The model correctly encodes the three-level hierarchy with monotonically increasing hyperbolic norms "fruit" is closest to the origin, "nut fruit" at moderate distance, and leaf nodes "filbert nut" and "common hazelnut" farthest from the origin. This demonstrates the model's ability to learn multi-level taxonomic structure from FoodOn training data.

HiM Untrained (Right): The randomly initialized model shows no hierarchical organization, nodes are scattered with inconsistent distance relationships.

Figure 11: Comparison of trained vs. untrained HiM embeddings on FoodOn hierarchy `fruit`→`nut fruit`→`{filbert, hazelnut}`. Trained model (left) preserves hierarchical distances; untrained model (right) shows random placement.

Figure 12: Out-of-distribution inference on hierarchy example from Figure 3. Root and intermediate levels are correctly ordered; leaf-level separation is reduced due to lack of training supervision for more specific entities.

G.2 Custom Hierarchy Inference: Figure 3 Concepts

To evaluate generalization to unseen entities, we tested the trained HiM-Poincaré model on the conceptual hierarchy from Figure 3: food→{desserts, appetizers}→{cheese cakes, crab cakes}. These exact entity names were not present in the FoodOn training ontology, requiring the model to infer hierarchical structure fr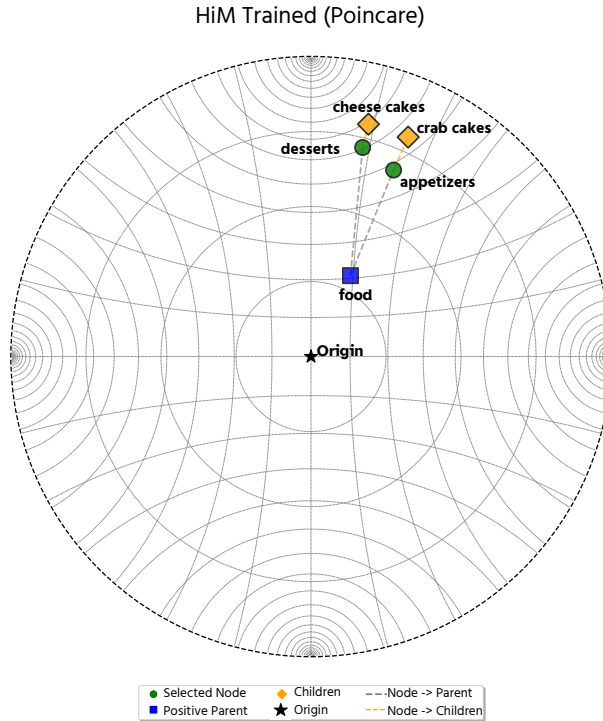om sentence embeddings. Figure 12 shows that the model successfully positions the root concept "food" closest to the origin (norm ≈ 0.30) and mid-level categories ("desserts", "appetizers") at intermediate distances (norms ≈ 0.85). The grandchildren nodes achieve similar norms (≈ 0.85-0.86) but are distinguished through angular separation, demonstrating that hyperbolic models can leverage both radial and angular dimensions when explicit hierarchical supervision is unavailable.

G.3 Visualization Methodology for Hyperbolic Embeddings

The 2D visualizations in Figure 2 and Appendix Figures 11–12 were generated using the following procedure:

1. Embedding Extraction: For a selected entity and its hierarchical neighbors (parent, children, negatives), we extracted their final 384-dimensional hyperbolic embeddings from the trained HiM-Poincaré model.

2. Dimensionality Reduction: We applied UMAP (McInnes et al., 2018) configured for hyperbolic geometry using the `umap-learn` library.

3. Projection: The 2D UMAP embeddings were re-projected onto the Poincaré disk using the exponential map to preserve hyperbolic distances.

4. Rendering: Visualizations use polar coordinates where radial position corresponds to hyperbolic norm and angular position follows UMAP embedding angles, rendered via `matplotlib` (Hunter, 2007).

This methodology ensures that the 2D projections respects the hyperbolic geometry, and the hierarchical depth correlates with radial distance from the origin.

H Additional Experimental Analysis

H.1 Larger pretrained LM baselines vs. HiM

To address concerns about whether the weak *pretrained* Euclidean baseline is primarily an effect of small parameter scale, we additionally report zero-shot **inference-only** results for substantially larger pretrained encoders, evaluated with the similar candidate-ranking protocol used for our Euclidean baselines. The evaluation protocol used in both mixed-hop prediction and multi-hop inference evaluates each child against one positive parent and multiple sampled negatives. Under this setting, zero-shot pretrained encoders frequently assign moderately high similarity scores to a large subset of candidates, resulting in inflated recall despite poor ranking fidelity. Consequently, several larger pretrained models exhibit near-saturated recall values while maintaining very low precision and F1 scores, indicating that the high recall is primarily driven by class imbalance rather than meaningful recovery of hierarchical parent relationships.

Table 6: Zero-shot inference baselines of larger pretrained encoders on hierarchical prediction/inference tasks, compared with HiM performance. Best per dataset column is bold; second-best is underlined (ties are broken deterministically to keep a single highlight per column). Metric: F1.

Model	Params (M)	doid-mixed	foodon-mixed	wordnet-mixed	wordnet-multi	snomed-mixed	snomed-multi
bert-base-uncased	110	0.155	0.128	0.197	0.201	0.173	0.176
bert-large-uncased	340	0.165	0.165	0.166	0.168	0.160	0.161
roberta-base	125	0.135	0.164	0.167	0.170	0.125	0.124
roberta-large	355	0.167	0.167	0.167	0.167	0.167	0.167
all-MiniLM-L6-v2	22	0.004	0.029	0.003	0.003	0.010	0.009
all-mpnet-base-v2	110	0.182	0.172	0.173	0.173	0.164	0.164
all-roberta-large-v1	355	0.167	0.167	0.167	0.167	0.167	0.167
HiM-Poincaré	16	<u>0.795</u>	**0.836**	**0.824**	<u>0.865</u>	<u>0.886</u>	<u>0.919</u>
HiM-Lorentz	16	**0.821**	<u>0.827</u>	<u>0.823</u>	**0.872**	**0.890**	**0.920**

Table 7: Same setting as Table 6; metric: Precision.

Model	Params (M)	doid-mixed	foodon-mixed	wordnet-mixed	wordnet-multi	snomed-mixed	snomed-multi
bert-base-uncased	110	0.092	0.159	0.132	0.135	0.101	0.103
bert-large-uncased	340	0.090	0.090	0.092	0.093	0.088	0.088
roberta-base	125	0.077	0.095	0.095	0.096	0.073	0.073
roberta-large	355	0.091	0.091	0.091	0.091	0.091	0.091
all-MiniLM-L6-v2	22	0.179	0.080	0.090	0.091	0.077	0.076
all-mpnet-base-v2	110	0.105	0.099	0.099	0.100	0.096	0.095
all-roberta-large-v1	355	0.091	0.091	0.091	0.091	0.091	0.091
HiM-Poincaré	16	<u>0.812</u>	<u>0.841</u>	**0.853**	<u>0.867</u>	<u>0.894</u>	<u>0.917</u>
HiM-Lorentz	16	**0.822**	**0.852**	<u>0.828</u>	**0.871**	**0.901**	**0.919**

Table 8: Same setting as Table 6; metric: Recall. High recall values reflect class imbalance in the candidate-ranking protocol (10:1 negatives-to-positive).

Model	Params (M)	doid-mixed	foodon-mixed	wordnet-mixed	wordnet-multi	snomed-mixed	snomed-multi
bert-base-uncased	110	0.496	0.107	0.387	0.392	0.578	0.606
bert-large-uncased	340	0.978	<u>0.972</u>	<u>0.874</u>	<u>0.883</u>	0.920	<u>0.927</u>
roberta-base	125	0.556	0.581	0.711	0.721	0.423	0.416
roberta-large	355	**0.993**	**0.993**	**0.994**	**0.994**	<u>0.992</u>	**0.993**
all-MiniLM-L6-v2	22	0.002	0.018	0.002	0.002	0.006	0.005
all-mpnet-base-v2	110	0.697	0.667	0.669	0.670	0.588	0.582
all-roberta-large-v1	355	<u>0.992</u>	0.993	0.994	0.994	**0.993**	0.993
HiM-Poincaré	16	0.780	0.831	0.798	0.863	0.877	0.921
HiM-Lorentz	16	0.820	0.803	0.815	0.872	0.880	0.920

H.2 Prompted LLM Experiment (GPT-4o vs. HiM)

To evaluate HiM's performance relative to contemporary large language models, we conducted a zero-shot evaluation using GPT-4o[3] on the WordNet mixed-hop prediction task. This comparison provides insight into how our specialized hyperbolic architecture performs against general-purpose language models that rely on vast pretraining but lack explicit hierarchical inductive biases. We generated 500 binary classification questions following the structure "Is [entity1] a subtype/subclass of [entity2]?" sampled from the same test set used for HiM evaluation. The experimental setup mirrored HiM's training regime: for each sampled child node, we generated one positive question and ten negative questions (corresponding to HiM's 1 positive parent + 10 hard negatives). GPT-4o was provided with a list of 74,401 WordNet entities as context and answered all 500 questions in a single zero-shot prompt without additional training. The results in Table 9 demonstrate that both HiM variants substantially outperform GPT-4o. GPT-4o performs well on general knowledge

---

[3]https://openai.com/index/hello-gpt-4o/

hierarchies where concepts like 'dog' → 'animal' are well-represented in large-scale training corpora. HiM (both Poincaré and Lorentz) still outperform GPT-4o by a clear margin, even on such general-knowledge hierarchy. The superior performance of HiM highlights the effectiveness of our hyperbolic modeling approach for hierarchical reasoning, even when compared to pretrained LLM with significantly larger parameter counts and extensive pretraining.

Table 9: F1 scores comparing HiM models with GPT-4o on WordNet mixed-hop prediction task

Dataset	HiM		GPT-4o
	Poincaré	Lorentz	
WordNet-mixed	0.859	0.850	0.750

H.3 Candidate-Selection Ranking Experiment (GPT-4o vs. HiM)

We evaluated GPT-4o using a candidate-selection/ranking methodology using similar evaluation strategy as HiM. Instead of free-form generation like in Appendix H.2, GPT-4o was presented with a list of candidate positive parents and negatives and tasked to select the correct hierarchical relationship. The comparison is presented in Table 10.

Table 10: Performance comparison between GPT-4o (candidate-ranking) and HiM models on mixed-hop prediction and multi-hop inference tasks.

Model	Dataset	F1	Precision	Recall
DOID Dataset (Average δ-hyperbolicity = 0.0190)				
GPT-4o	doid-mixed	**0.834**	**0.834**	**0.834**
HiM-Poincaré	doid-mixed	0.795	0.812	0.780
HiM-Lorentz	doid-mixed	0.821	0.822	0.820
FoodOn Dataset (Average δ-hyperbolicity = 0.1852)				
GPT-4o	foodon-mixed	0.539	0.540	0.539
HiM-Poincaré	foodon-mixed	**0.836**	0.841	**0.831**
HiM-Lorentz	foodon-mixed	0.827	**0.852**	0.803
WordNet Dataset (Mixed-hop, δ-hyperbolicity = 0.1438)				
GPT-4o	wordnet-mixed	0.550	0.550	0.550
HiM-Poincaré	wordnet-mixed	**0.824**	**0.853**	0.798
HiM-Lorentz	wordnet-mixed	0.823	0.828	**0.815**
WordNet Dataset (Multi-hop, δ-hyperbolicity = 0.1431)				
GPT-4o	wordnet-multi	0.516	0.516	0.516
HiM-Poincaré	wordnet-multi	0.865	0.867	0.863
HiM-Lorentz	wordnet-multi	**0.872**	**0.871**	**0.872**

GPT-4o achieves competitive performance on the DOID dataset, likely due to its relatively small size and low δ-hyperbolicity (0.0190), which indicates a near tree-like structure that aligns well with semantically descriptive biomedical terminology present in the model's pretraining corpus. However, HiM models substantially outperform GPT-4o on FoodOn and WordNet. While GPT-4o benefits from extensive semantic knowledge, it lacks the geometric inductive bias required to consistently encode hierarchical distances and transitivity constraints. In contrast, HiM explicitly learns these structural relationships through geometry-aware training, enabling more robust hierarchical reasoning across ontologies, even under a candidate-selection evaluation aligned with embedding-based ranking.

H.4 Computational Efficiency Analysis

To substantiate our claims regarding Mamba's linear complexity advantages, we conducted a sequence length scaling study on the WordNet dataset for the mixed-hop prediction task. The results in Table 11 validate Mamba's theoretical linear complexity characteristics. Doubling the sequence length from 128 to 256 tokens results in an exact $2\times$ increase in both FLOPs ($4.46\text{G} \rightarrow 8.9\text{G}$) and MACs ($2.23\text{G} \rightarrow 4.45\text{G}$), while memory consumption remains constant at 66.91MB due to the fixed number of model parameters and activations. This linear scaling behavior contrasts sharply with transformer-based architectures, where sequence length increases would result in quadratic growth in computational requirements.

Table 11: Sequence length scaling analysis for HiM-16M-Poincaré on WordNet mixed-hop prediction

Sequence Length	FLOPs	MACs	Memory	Training Time
128	4.46 G	2.23 G	66.91 MB	0:41:32
256	8.90 G	4.45 G	66.91 MB	0:42:13

I Ablation Studies

We conducted systematic ablation studies to validate key design choices in HiM architecture. All ablations were performed on WordNet-mixed and DOID-mixed tasks using the default HiM configuration. Results are reported as mean $\pm$ standard deviation over 5 independent runs.

I.1 Loss Component Ablation

We evaluated six loss configurations with varying margin ratios (α, β) where margins scale with hyperbolic radius R:

- **original** $(0.255 \cdot R, 0.0051 \cdot R)$: Our default balanced configuration
- **only_clustering** $(0.255 \cdot R, 0.0)$: Clustering loss only (no parent-child ordering)
- **only_centripetal** $(0.0, 0.0051 \cdot R)$: Centripetal loss only (no entity separation)
- **high_clustering** $(0.510 \cdot R, 0.0051 \cdot R)$: Doubled clustering margin
- **high_centripetal** $(0.255 \cdot R, 0.0102 \cdot R)$: Doubled centripetal margin
- **standard_contrastive** $(0.051R, 0.0)$: Euclidean triplet loss

Table 12: Loss component ablation on WordNet-mixed and DOID-mixed. Standard contrastive loss (Euclidean triplet) shows substantial degradation, confirming the necessity of hyperbolic-specific losses.

Loss Configuration	WordNet-mixed		DOID-mixed	
	Poincaré (F1)	Lorentz (F1)	Poincaré (F1)	Lorentz (F1)
original	**0.843 ± 0.007**	0.843 ± 0.001	**0.811 ± 0.008**	**0.823 ± 0.015**
only_clustering	0.842 ± 0.011	0.844 ± 0.003	0.786 ± 0.021	0.813 ± 0.021
only_centripetal	0.817 ± 0.005	0.808 ± 0.005	0.775 ± 0.038	0.790 ± 0.010
high_clustering	0.833 ± 0.005	**0.845 ± 0.005**	0.797 ± 0.010	0.798 ± 0.014
high_centripetal	0.839 ± 0.011	0.843 ± 0.001	0.810 ± 0.008	0.809 ± 0.025
standard_contrastive	0.452 ± 0.085	0.605 ± 0.042	0.197 ± 0.020	0.264 ± 0.012

Results in Table 12 demonstrate that the original balanced configuration achieves competitive performance across both manifolds. Critically, standard_contrastive loss performs substantially worse, demonstrating that Euclidean triplet losses are fundamentally unsuitable for hyperbolic embeddings due to the mismatch between flat Euclidean geometry and negatively curved hyperbolic space. Using only_clustering

or only_centripetal may slightly reduces performance, supporting that both components contribute complementarily: clustering enforces entity separation while centripetal preserves parent-child hierarchy. Notably, high_clustering achieves the best Lorentz performance on WordNet, suggesting that stronger negative separation may benefit deeper hierarchies in unbounded manifold.

I.2 Pooling Strategy Ablation

We compared three pooling strategies to aggregate Mamba2 sequence outputs: (1) **Mean**: averaging all token embeddings (our default), (2) **Max**: element-wise maximum over sequence, (3) **Last Token**: using final position embedding (analogous to transformer CLS tokens, but leveraging Mamba's causal autoregressive accumulation rather than a dedicated token).

Table 13: Pooling strategy ablation. Mean pooling achieves best overall performance; last token is competitive on WordNet-Lorentz due to Mamba's autoregressive state accumulation.

Pooling	WordNet-mixed		DOID-mixed	
	Poincaré (F1)	Lorentz (F1)	Poincaré (F1)	Lorentz (F1)
Mean	**0.843 ± 0.007**	0.843 ± 0.001	**0.811 ± 0.008**	**0.823 ± 0.015**
Max	0.833 ± 0.006	0.833 ± 0.005	0.794 ± 0.007	0.726 ± 0.057
Last Token	0.843 ± 0.006	**0.844 ± 0.008**	0.802 ± 0.020	0.806 ± 0.011

Results in Table 13 show that mean pooling achieves the best overall performance. Last token pooling performs comparably on WordNet (F1=0.844 for Lorentz), reflecting Mamba's autoregressive nature where final states accumulate the entire sequence information. Max pooling consistently underperforms, likely because max operations can amplify outlier features unsuitable for hierarchical distance computation. These findings validate our default choice of mean pooling.

I.3 Model Depth Ablation

We evaluated 2, 4, and 6 Mamba2 layers while keeping other hyperparameters fixed (d_model=384, d_state=128, expand=4). The 6-layer configuration underperforms across both datasets. This suggests that excessive depth is unnecessary for capturing hierarchical structure when combined with hyperbolic geometry.

Table 14: Model depth ablation. 2-4 layers offer optimal capacity; 6 layers show overfitting on moderately-sized ontologies.

Layers	WordNet-mixed		DOID-mixed	
	Poincaré (F1)	Lorentz (F1)	Poincaré (F1)	Lorentz (F1)
2	**0.844 ± 0.007**	**0.843 ± 0.002**	0.805 ± 0.009	0.802 ± 0.026
4	0.843 ± 0.007	0.843 ± 0.001	**0.811 ± 0.008**	**0.823 ± 0.015**
6	0.834 ± 0.006	0.833 ± 0.006	0.799 ± 0.005	0.779 ± 0.000

I.4 Negative Sampling Ablation

We compared **hard negative mining** (selecting semantically similar siblings/cousins) against **random negative sampling** (uniformly sampling unrelated entities). Results in Table 15 show mixed outcomes, hard negatives improve WordNet performance, likely due to WordNet's complex multi-level hierarchy requiring fine-grained discrimination. However, on DOID, random negatives perform better, possibly because DOID's is smaller dataset where random negatives themselves provide sufficient separation.

Table 15: Negative sampling ablation. Hard negatives improve complex hierarchies (WordNet) but show mixed results on smaller datasets (DOID).

Sampling	WordNet-mixed		DOID-mixed	
	Poincaré (F1)	Lorentz (F1)	Poincaré (F1)	Lorentz (F1)
Hard Negative	**0.843 ± 0.007**	**0.843 ± 0.001**	0.808 ± 0.005	0.823 ± 0.015
Random Negative	0.828 ± 0.016	0.841 ± 0.009	**0.839 ± 0.022**	**0.852 ± 0.023**

J   Model Size Configurations

To investigate the effect of model capacity on hierarchical reasoning performance, we scaled our HiM architecture from 16M to 32M parameters. Table 16 details the complete hyperparameter configuration for both model scales. We kept the base hidden dimension (`d_model` = 384), state dimension (`d_state` = 128), and convolution kernel size (`d_conv` = 7) constant to maintain consistency in the input/output interfaces and local temporal modeling.

Table 16: Hyperparameter configuration for 16M and 32M parameter models. Scaling is achieved through combined depth (n_layer) and width (expand, headdim) increases.

Hyperparameter	16M	32M
`d_model` (Hidden Dim)	384	384
`n_layer` (Depth)	3	7
`d_state` (State Dim)	128	128
`d_conv` (Conv Kernel)	7	7
`expand` (Expansion Factor)	4	6
`headdim` (Head Dim)	96	128
Total Parameters	**~16M**	**~32M**

K   Code Availability

The source code for the Hierarchical Mamba (HiM) model is publicly available at `https://anonymous.4open.science/r/HiM-3202` with detailed instructions for setup and execution.

L   Declaration of LLM usage

LLMs were only used to assist with writing and formatting, not as part of the core methodology. Large Language Models (LLMs) were used in a limited capacity during the preparation of this manuscript for grammar checking and text refinement. All technical contributions, results and insights are the original work of the authors.